Draft version January 14, 2015
Preprint typeset using LaTeX style emulateapj v. 05/12/14

arXiv:1410.8138v2 [astro-ph.SR] 12 Jan 2015

A NEW CLASS OF NASCENT ECLIPSING BINARIES WITH EXTREME MASS RATIOS

Maxwell Moe[1] & Rosanne Di Stefano[1]

Draft version January 14, 2015

ABSTRACT

Early B-type main-sequence (MS) stars ($M_1 \approx 5$ - $16\,M_\odot$) with closely orbiting low-mass stellar companions ($q = M_2/M_1 < 0.25$) can evolve to produce Type Ia supernovae, low-mass X-ray binaries, and millisecond pulsars. However, the formation mechanism and intrinsic frequency of such close extreme mass-ratio binaries have been debated, especially considering none have hitherto been detected. Utilizing observations of the Large Magellanic Cloud galaxy conducted by the Optical Gravitational Lensing Experiment, we have discovered a new class of eclipsing binaries in which a luminous B-type MS star irradiates a closely orbiting low-mass pre-MS companion that has not yet fully formed. The primordial pre-MS companions have large radii and discernibly reflect much of the light they intercept from the B-type MS primaries ($\Delta I_{\rm refl} \approx 0.02$ - 0.14 mag). For the 18 definitive MS + pre-MS eclipsing binaries in our sample with good model fits to the observed light curves, we measure short orbital periods $P = 3.0$ - 8.5 days, young ages $\tau \approx 0.6$ - 8 Myr, and small secondary masses $M_2 \approx 0.8$ - $2.4\,M_\odot$ ($q \approx 0.07$ - 0.36). The majority of these nascent eclipsing binaries are still associated with stellar nurseries, e.g. the system with the deepest eclipse $\Delta I_1 = 2.8$ mag and youngest age $\tau = 0.6 \pm 0.4$ Myr is embedded in the bright H II region 30 Doradus. After correcting for selection effects, we find that $(2.0 \pm 0.6)\%$ of B-type MS stars have companions with short orbital periods $P = 3.0$ - 8.5 days and extreme mass ratios $q \approx 0.06$ - 0.25. This is $\approx$10 times greater than that observed for solar-type MS primaries. We discuss how these new eclipsing binaries provide invaluable insights, diagnostics, and challenges for the formation and evolution of stars, binaries, and H II regions.

Subject headings: binaries: eclipsing, close; stars: massive, pre-main sequence, formation, evolution, statistics; ISM: H II regions, evolution; galaxies: Large Magellanic Cloud

1. INTRODUCTION

Close binaries with orbital periods $P \lesssim 10^3$ days are ubiquitous (Abt 1983; Duquennoy & Mayor 1991; Kobulnicky & Fryer 2007; Raghavan et al. 2010; Sana et al. 2012; Duchêne & Kraus 2013) and are the progenitors of a variety of astrophysical phenomena (Paczyński 1971; Iben & Tutukov 1987; Verbunt 1993; Phinney & Kulkarni 1994; Taam & Sandquist 2000). Nonetheless, a close stellar companion cannot easily form in situ (see Mathieu 1994 and Tohline 2002 for observational and theoretical reviews, respectively). Instead, the companion most likely fragments from the natal gas cloud or circumstellar disk at initially wider orbital separations (Bate & Bonnell 1997; Kratter & Matzner 2006). Various migration hypotheses have been proposed for how the orbit decays to shorter periods (Bate et al. 2002; Bonnell & Bate 2005). These formation scenarios produce mostly close binaries with components of comparable mass because a low-mass companion either accretes additional mass from the disk, merges with the primary, remains at wide separations, or is dynamically ejected from the system.

Close binaries with extreme mass ratios most likely require an alternative formation mechanism. For example, a low-mass companion can be tidally captured into a closer orbit (Press & Teukolsky 1977; Bally & Zinnecker 2005; Moeckel & Bally 2007), possibly with the assistance of gravitational perturbations from a third star (Kiseleva et al. 1998; Naoz & Fabrycky 2014). Indeed, a significant fraction of close binaries are orbited by an outer tertiary (Tokovinin et al. 2006), suggesting the third star may play a role in the dynamical formation of the system. It is fair to say that the mutual formation and coevolution between massive stars and close companions are not yet fully understood. It has even been proposed that massive stars formed primarily via mergers of close binaries instead of through gas accretion from the circumstellar disk (Bonnell & Bate 2005; Bally & Zinnecker 2005). A complete census of close companions to massive stars must be conducted in order to determine the dominant formation mechanism of close binaries and massive stars as well as to reliably predict the production rates of certain channels of binary evolution.

It is extremely difficult, however, to detect faint low-mass companions that are closely orbiting massive luminous primaries. B-type main-sequence (MS) stars with low-mass secondaries have been photometrically resolved at extremely wide orbital separations $a \gtrsim 50$ AU, i.e. long orbital periods $P \gtrsim 10^5$ days (Abt et al. 1990; Shatsky & Tokovinin 2002). Some of these resolved low-mass companions are still pre-MS stars that can emit X-rays (Hubrig et al. 2001; Stelzer et al. 2003). Late B-type MS stars detected at X-ray wavelengths most likely have unresolved low-mass pre-MS companions at $a \lesssim 50$ AU (Evans et al. 2011). However, the precise orbital periods of these putative X-ray emitting companions have not yet been determined. These unresolved binaries may

[1] Harvard-Smithsonian Center for Astrophysics, 60 Garden Street, MS-10, Cambridge, MA, 02138, USA; e-mail: mmoe@cfa.harvard.edu

have short orbital periods $P < 10^3$ days and may eventually experience substantial mass transfer and/or common envelope evolution as the primary evolves off the MS. Alternatively, the binaries could have intermediate orbital periods $P = 10^3$ - 10^5 days and could therefore avoid Roche-lobe overflow.

Multi-epoch radial velocity observations of double-lined spectroscopic binaries (SB2s) can provide the orbital periods P and velocity semi-amplitudes K_1 and K_2. Hence, the mass ratio $q \equiv M_2/M_1 = K_1/K_2$ of an SB2 can be directly measured dynamically. However, SB2s with MS components can only reveal companions that are comparable in luminosity, and therefore mass, to the primary star. SB2s with early-type primaries, known orbital periods, and dynamically measured masses all have moderate mass ratios $q > 0.25$ (Wolff 1978; Levato et al. 1987; Abt et al. 1990; Sana et al. 2012). Gullikson & Dodson-Robinson (2013) combined multiple high-resolution spectra of early-type stars in order to substantially increase the signal-to-noise. By implementing this novel technique, they detected SB2s with larger luminosity contrasts and therefore smaller mass ratios $q \approx 0.1$ - 0.2. Although Gullikson & Dodson-Robinson (2013) found a few candidates, stacking multiple spectra from random epochs in order to increase the signal-to-noise does not relay the orbital period of the binary. Similar to the case above of late-B primaries with unresolved, X-ray emitting companions, these SB2s with indeterminable periods may have wide orbital separations.

Close faint companions to B-type MS primaries can induce small radial velocity variations, and these reflex motions have been observed with multi-epoch spectroscopy (Wolff 1978; Levato et al. 1987; Abt et al. 1990). Although the orbital periods of these single-lined spectroscopic binaries (SB1s) can be measured, they have only lower limits for their mass ratios because the inclinations are not known. Nonetheless, an average inclination or a distribution of inclinations can be assumed for a population of SB1s in order to recover a statistical mass-ratio distribution (Mazeh & Goldberg 1992). For SB1s with solar-type MS primaries $M_1 \approx 1\,M_\odot$, the companions are almost certainly low-mass M-dwarfs (Duquennoy & Mayor 1991; Mazeh et al. 1992; Grether & Lineweaver 2006; Raghavan et al. 2010). For early-type MS primaries $M_1 \approx 10\,M_\odot$, however, SB1s can either contain $M_2 \approx 0.5$ - $3\,M_\odot$ K-A type stellar companions or $M_2 \approx 0.5$ - $3\,M_\odot$ stellar remnants such as white dwarfs, neutron stars, or black holes (Wolff 1978; Garmany et al. 1980). Wolff (1978) even suggests that most SB1s with late-B MS primaries contain white dwarf companions, and therefore the fraction of unevolved low-mass stellar companions to B-type MS stars is rather small. Unfortunately, there is at present no easy and systematic method for distinguishing between these two possibilities for all SB1s in a statistical sample. Because early-type SB1s may be contaminated by evolved stellar remnants, it is prudent to only consider binaries where the nature of the secondaries are reliably known. In addition to discovering close unevolved low-mass companions to B-type MS stars, we must also utilize a different observational technique for easily identifying such systems from current and future telescopic surveys.

Fortunately, extensive visual monitoring of one of our satellite galaxies, the Large Magellanic Cloud (LMC), conducted by the third phase of the Optical Gravitational Lensing Experiment (OGLE-III) has yielded a vast database primed for the identification and analysis of such binaries (Udalski et al. 2008; Graczyk et al. 2011). OGLE-III surveyed 35 million stars in the LMC over seven years, typically obtaining $\approx$470 near-infrared I and $\approx$45 visual V photometric measurements per star (Udalski et al. 2008). Moreover, Graczyk et al. (2011) utilized a semi-automated routine to identify more than 26,000 eclipsing binaries in the OGLE-III LMC database. They cataloged basic observed parameters of the eclipsing binaries such as orbital periods P and primary eclipse depths ΔI_1, but the intrinsic physical properties of the eclipsing binaries still need to be quantified.

We previously showed that B-type MS stars with low-mass zero-age MS companions $q \approx 0.1$ - 0.2 can produce shallow eclipses $\Delta I_1 \approx 0.1$ - 0.2 mag if the inclinations are sufficiently close to edge-on (see Fig. 5 in Moe & Di Stefano 2013). Indeed, the OGLE-III LMC survey is sensitive to such shallow eclipses, so we expect B-type MS stars with low-mass companions to be hiding in the OGLE-III LMC eclipsing binary catalog. We therefore began to systematically measure the physical properties of the eclipsing binaries in hopes of identifying such extreme mass-ratio binaries.

While investigating the light curves of eclipsing binaries in the OGLE-III LMC database, we serendipitously discovered an unusual subset that displayed sinusoidal profiles between narrow eclipses (prototype shown in Fig. 1). We soon realized the sinusoidal variations are caused by the reflection of light received by a large, low-mass, *pre-MS* companion from the hot B-type MS primary. The present study is dedicated to a full multi-stage analysis of this new class of eclipsing binaries. In §2, we present our selection criteria for identifying "reflecting" eclipsing binaries with B-type MS stars and low-mass pre-MS companions. We then measure the physical properties of these systems by fitting eclipsing binary models to the observed light curves (§3). We also examine observed correlations among various properties of our nascent eclipsing binaries, including their associations with star-forming H II regions (§4). In §5, we correct for selection effects in order to determine the intrinsic frequency of close, low-mass companions to B-type MS stars. In §6, we discuss the implications of these eclipsing binaries in the context of binary star formation and evolution. Finally, we summarize our main results and conclusions (§7).

2. A NEW CLASS OF ECLIPSING BINARIES

2.1. *Selection Criteria and Analytic Models*

The OGLE-III LMC photometric database (Udalski et al. 2008) lists the mean magnitudes $\langle I \rangle$, colors $\langle V - I \rangle$, and positions for each of the 35 million stars in their survey. Throughout this work, we adopt a distance $d = 50$ kpc to the LMC (Pietrzyński et al. 2013). We also incorporate stellar parameters such as temperature-dependent bolometric corrections

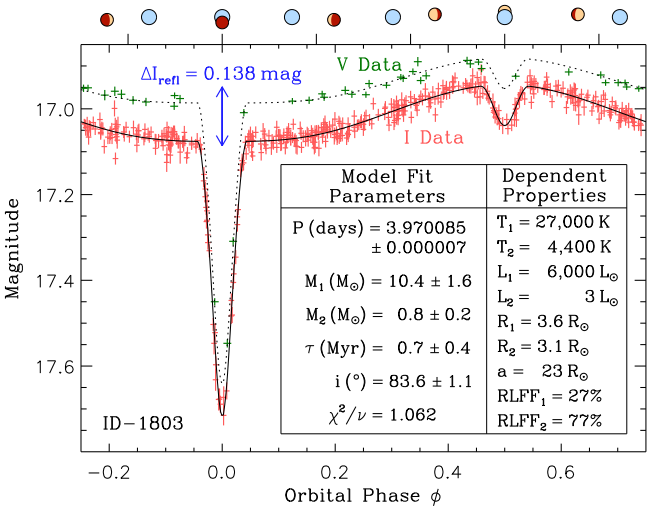

FIG. 1.— One of the 22 OGLE-III LMC eclipsing binary light curves with a B-type MS primary and low-mass pre-MS companion. We fit a detailed *physical* model (black; see §3 for details) to the V-band data (green) and I-band data (red). The large reflection effect amplitude $\Delta I_{\rm refl}$ (blue) is used to identify such systems (see §2). Above is a to-scale schematic diagram of the binary at the orbital phases indicated by the tick marks. The narrow eclipses dictate a detached binary configuration with Roche-lobe fill-factors $RLFF < 80\%$, which indicate both components are effectively evolving along their respective single-star sequences. The inset tables show the main parameters constrained by the physical model fit (left), and the dependent properties (right) derived by using the model parameters in combination with Kepler's laws and stellar evolutionary tracks. The reported uncertainties in the physical model parameters are dominated by the systematic uncertainties in the stellar evolutionary tracks. Because the distances to eclipsing binaries in the LMC are known, the photospheric properties are reliably measured from the observed light curve features, e.g. ≈8% uncertainties in the temperatures, ≈40% uncertainties in the luminosities, and ≈10% uncertainties in the radii, separation, and Roche-lobe fill-factors. Note the extreme mass ratio $q = M_2/M_1 = 0.07$, young age, and how the primary B-type MS star is significantly hotter and more luminous than the pre-MS secondary.

BC($T_{\rm eff}$) and intrinsic color indices $(V-I)_{\rm o}\,(T_{\rm eff})$ from Pecaut & Mamajek (2013). Based on these parameters, we select the $\mathcal{N}_{\rm B} \approx 174{,}000$ systems from the OGLE-III LMC catalog with mean magnitudes $16.0 < \langle I \rangle < 18.0$ and colors $-0.25 < \langle V-I \rangle < 0.20$ that correspond to luminosities and surface temperatures, respectively, of B-type MS stars.

The OGLE-III LMC eclipsing binary catalog (Graczyk et al. 2011) provides the time t, photometric magnitude I or V, and photometric error $\sigma_{\rm phot}$ for the $\mathcal{N}_I \approx 470$ and $\mathcal{N}_V \approx 45$ measurements of each eclipsing binary. It also gives general properties of each eclipsing binary such as the orbital period P (in days) and epoch of primary eclipse minimum $t_{\rm o}$ (Julian Date − 2450000). The orbital phase simply derives from folding the time of each measurement with the orbital period:

$$\phi(t) = \frac{(t - t_{\rm o}) \bmod P}{P}. \qquad (1)$$

We analyze the 2,206 OGLE-III LMC eclipsing binaries that have orbital periods $P = 3$ - 15 days and satisfy our magnitude and color criteria. Such an immense sample of close companions to B-type MS stars is two orders of magnitude larger than previous spectroscopic binary surveys (Wolff 1978; Levato et al. 1987; Abt et al. 1990).

To automatically and robustly identify "reflecting" eclipsing binaries, we fit an analytic model of Gaussians and sinusoids to the I-band light curves for each of the 2,206 eclipsing binaries in our full sample. The parameters are as follows. The average magnitude $\langle I \rangle$ is the total I-band magnitude of both stars if they did not exhibit eclipses or reflection effects. The primary and secondary eclipse depths are ΔI_1 and ΔI_2, and the primary and secondary eclipse widths are Θ_1 and Θ_2, respectively. The phase of the secondary eclipse Φ_2 provides a lower limit to the eccentricity of the orbit (Kallrath & Milone 2009):

$$e \geq e_{\rm min} = |e\cos(\omega)| = \pi|\Phi_2 - 1/2|/2, \qquad (2)$$

where ω is the argument of periastron. Finally, $\Delta I_{\rm refl}$ is the full amplitude of the reflection effect, which unlike eclipses, leads to an increase in brightness. With these definitions, we model the I-band light curves in terms of Gaussians and sinusoids:

$$\begin{aligned} I_{\rm GS}(\phi) = \langle I \rangle &+ \Delta I_1 \Big[\exp\Big(\frac{-\phi^2}{2\Theta_1^2}\Big) + \exp\Big(\frac{-(\phi-1)^2}{2\Theta_1^2}\Big)\Big] \\ &+ \Delta I_2 \exp\Big(\frac{-(\phi-\Phi_2)^2}{2\Theta_2^2}\Big) \\ &- \frac{\Delta I_{\rm refl}}{2}\Big[\cos\big(2\pi[\phi - 1/2]\big) + 1\Big]. \end{aligned} \qquad (3)$$

The photometric errors $\sigma_{\rm phot}$ provided in the catalog systematically underestimate the true rms dispersion outside of eclipse by (5 - 20)% (see Fig. 2). This is especially true for the brightest systems $\langle I \rangle \approx 16.0$ - 16.5 where the photometric errors $\sigma_{\rm phot} \approx 0.008$ mag are small. We separately fit 3rd degree polynomials across the out-of-eclipse intervals $3\Theta_1 < \phi < \Phi_2 - 3\Theta_2$ and $\Phi_2 + 3\Theta_2 < \phi < 1 - 3\Theta_1$ for the eclipsing binaries with at least 50 data points across these intervals. We then measure the rms dispersion $\sigma_{\rm rms}$ of the residuals resulting from these fits. To rectify the differences between the catalog and actual errors, we multiply each of the photometric uncertainties by a correction factor f_σ:

$$\sigma_{\rm corr}(t) = \sigma_{\rm phot}(t) f_\sigma, \qquad (4)$$

where f_σ increases toward brighter systems:

$$f_\sigma(I) = 1.05 + 0.15 \times 10^{(16.0-I)/2}. \qquad (5)$$

The source of this systematic error could partially be due to intrinsic variations in the luminosities of B-type MS stars at the 0.5% level. In any case, the corrected total errors $\sigma_{\rm corr}$ follow the measured rms errors $\sigma_{\rm rms}$ quite well (Fig. 2). We implement these corrected errors $\sigma_{\rm corr}$ in our analytic light curve models below.

Even after accounting for the systematic error correction factor f_σ, a few of the photometric measurements are clear outliers. We therefore clip up to $\mathcal{N}_{\rm c} \leq 2$ measurements per light curve that deviate more than 4σ from our best-fit model. To be conservative, we only eliminate up to two data points to ensure we did not remove any intrinsic signals. Our analytic model has nine parameters (seven explicitly written in Eq. 3 as well

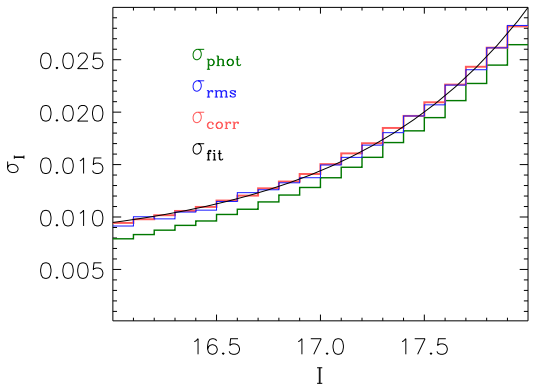

FIG. 2.— For each interval of I-band magnitudes, we compare the median values of the photometric errors $\sigma_{\rm phot}$ reported in the OGLE-III LMC eclipsing binary catalog (green), the intrinsic rms variations $\sigma_{\rm rms}$ outside of eclipse (blue), and the total corrected errors $\sigma_{\rm corr}$ (red). We also display a fit $\sigma_{\rm fit}$ (black) to the total errors.

as our own fitted values of P and $t_{\rm o}$ according to Eq. 1), which provide $\nu = \mathcal{N}_I - \mathcal{N}_{\rm c} - 9$ degrees of freedom.

For the 2,206 eclipsing binaries, we use an automated Levenberg-Marquardt technique to minimize the $\chi^2_{\rm GS}$ statistic between the light curves and analytic models. We also calculate the covariance matrix and standard 1σ statistical uncertainties for our nine fitted parameters. We visually inspect the solutions for all systems with $\chi^2_{\rm GS}/\nu > 1.5$ to ensure the parameters converged to the best possible values. For the few models that automatically converged to a local non-global minimum, we adjusted the initial fit parameters and reiterated the Levenberg-Marquardt technique to determine the lowest $\chi^2_{\rm GS}/\nu$ value possible.

Our analytic model of Gaussians and sinusoids does not adequately describe some of the eclipsing binaries, which can lead to large values of $\chi^2_{\rm GS}/\nu = 2\text{-}5$. For example, some of our systems with nearly edge-on orientations exhibit flat-bottomed eclipses, and therefore a simple Gaussian does not precisely match the observed eclipse profile. In addition, our analytic model cannot reproduce light curves with extreme ellipsoidal modulations, i.e. systems with tidally deformed and oblate stars. Nonetheless, our analytic model captures the basic light curve parameters of eclipse depths, eclipse widths, eclipse phases, and amplitude of the reflection effect. These parameters are sufficient in allowing us to distinguish different classes of eclipsing binaries.

To identify eclipsing binaries with reflection effects and well-defined eclipses, we impose the following selection criteria. We require the reflection effect amplitude to be $\Delta I_{\rm refl} > 0.015$ mag and its 1σ uncertainty to be <20% of its value. We stipulate that the 1σ uncertainties in the eclipse depths ΔI_1 and ΔI_2 and eclipse widths Θ_1 and Θ_2 are <25% their respective values. We discard eclipsing binaries with wide eclipses $\Theta_{\rm max} = \max(\Theta_1, \Theta_2) > 0.05$, which removes most systems that have filled their Roche lobes, e.g. semi-detached and contact binaries. Eclipsing binaries with shallow eclipse depths can remain undetected given the sensitivity and cadence of the OGLE-III LMC observations. We therefore keep only systems with total light curve amplitudes:

$$\Delta I = \Delta I_1 + \Delta I_{\rm refl} \geq 10^{0.2(\langle I \rangle - 16.0)} \times 0.08\,{\rm mag} \qquad (6)$$

to ensure our sample is complete in our selected parameter space (see detection limits in Fig. 3 of Graczyk et al. 2011).

2.2. *Results*

We find 90 eclipsing binaries that satisfy these initial selection criteria (see Fig. 3). In this subsample, there is one semi-detached binary (magenta system in Fig. 3) and 51 Algols, i.e. evolved semi-detached eclipsing binaries that have inverted their mass ratios via stable mass transfer (red population in Fig. 3). These evolved eclipsing binaries have wide eclipses $0.031 < \Theta_{\rm max} < 0.050$ that dictate at least one of the binary components fills their Roche lobe. Previous studies of eclipsing binaries in the LMC have noted this Algol population by identifying systems with wide eclipses and large temperature contrasts (Mazeh et al. 2006; Prša et al. 2008).

The remaining 38 objects that satisfy our initial selection criteria have intriguing light curves. We list their catalog properties and analytic light curve parameters in Table 1. All but one of these eclipsing binaries have $\Theta_{\rm max} < 0.028$, which indicate a detached configuration. In the following, we use the measured analytic parameters of these 38 systems to understand their physical properties as well as to distinguish various classes of eclipsing binaries.

2.2.1. *MS + Pre-MS "Reflecting" Eclipsing Binaries with Extreme Mass Ratios*

Of the 38 unusual eclipsing binaries, we discover that 22 systems form a distinct population with definitive reflection effects $\Delta I_{\rm refl} > 0.015$ mag, narrow eclipses $\Theta_{\rm max} < 0.03$, relatively shallow secondary eclipses $\Delta I_2/\Delta I_1 < 0.4$, and nearly circular orbits according to Φ_2 and Eq. 2 (blue systems in Fig. 3). These 22 eclipsing binaries have short orbital periods $P = 3.0\text{-}8.5$ days, large reflection effect amplitudes $\Delta I_{\rm refl} = 0.017\text{-}0.138$ mag, and moderate to deep primary eclipses $\Delta I_1 = 0.09\text{-}2.8$ mag.

The reflection effects and primary eclipse depths can be so prominent only if the companions are comparable in size to but substantially cooler than the B-type MS primaries. The companions cannot be normal MS stars since cooler MS stars are also considerably smaller. We can eliminate the alternative that the companions are evolved cool subgiants in an Algol binary because such large subgiants fill their Roche lobes and produce markedly wider eclipses. We therefore conclude that the companions in our 22 systems are cool medium-sized low-mass pre-MS stars that have not yet fully formed.

We can observe these nascent B-type MS + low-mass pre-MS eclipsing binaries at such a special time in their evolution because low-mass companions $q \lesssim 0.25$ contract considerably more slowly during their pre-MS phase of formation. See §3, where we more thoroughly analyze the physical properties of these systems by fitting detailed physical light curve models. Our 22 eclipsing binaries with pronounced reflection effects therefore constitute a new class of detached MS + pre-MS close binaries with extreme mass ratios. These systems also represent the first unambiguous identification of B-type MS stars with closely orbiting low-mass stellar companions.

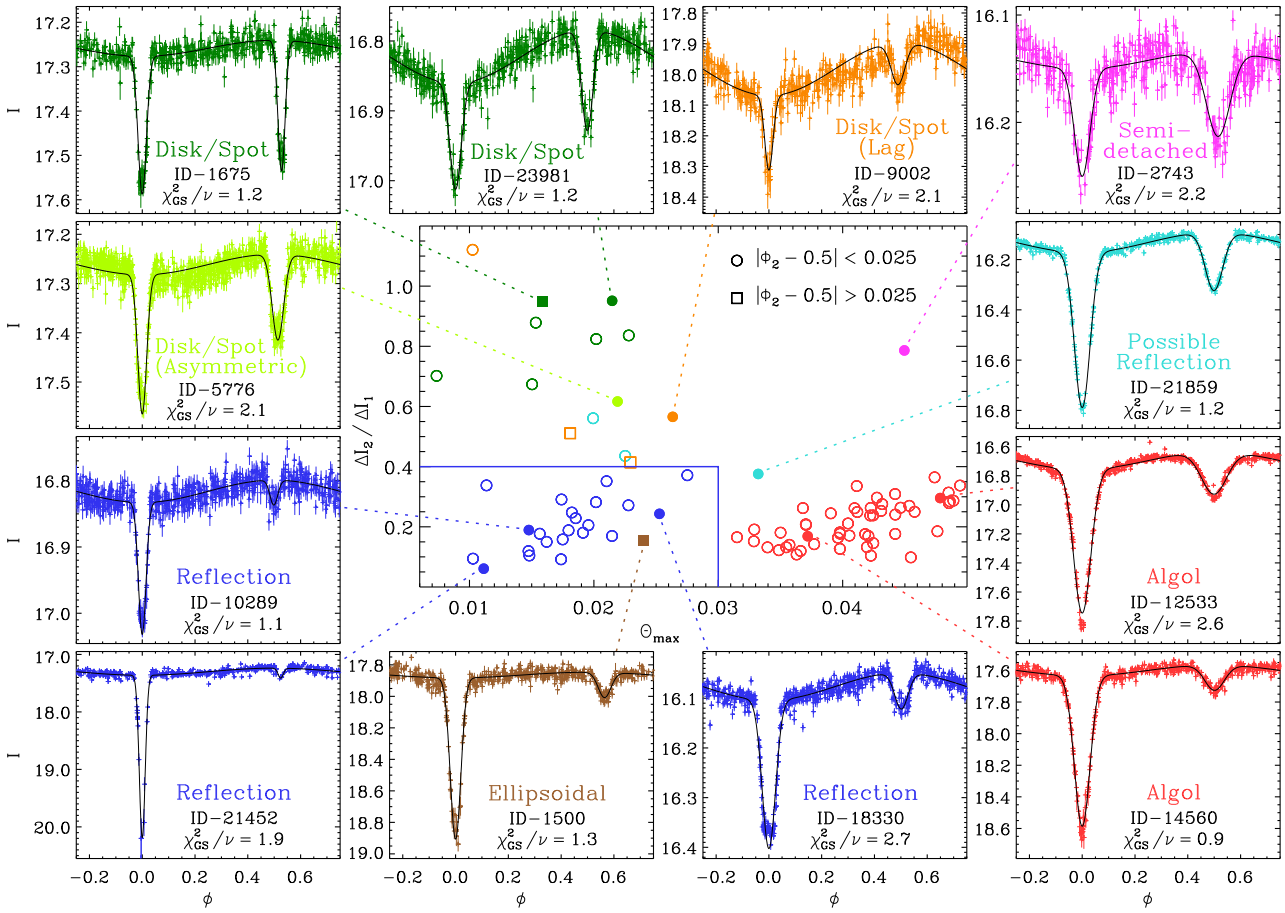

FIG. 3.— Outside panels: Example light curves of the various eclipsing binary populations and the best *analytic* fits of Gaussians and sinusoids. Center panel: Ratio of eclipse depths $\Delta I_2/\Delta I_1$ versus maximum eclipse width $\Theta_{\rm max} = \max(\Theta_1, \Theta_2)$ for the 90 eclipsing binaries with B-type MS primaries, P = 3 - 15 days, $\Delta I_{\rm refl} > 0.015$ mag, and $\Theta_{\rm max} < 0.05$. Eclipsing binaries with components of comparable luminosity are toward the top and those with a component that fills or nearly fills its Roche lobe are toward the right. We also distinguish systems with eccentric orbits $e > e_{\rm min} > 0.04$ (square symbols) from those that most likely have nearly circular orbits (circles) based on the observed orbital phase of the secondary eclipse Φ_2. Dotted lines and filled symbols match each light curve to the corresponding system in the central panel. A semi-detached binary (magenta) is to the upper right. Evolved semi-detached Algols (red) with broad eclipse features, large temperature contrasts, and inverted mass ratios are to the bottom right. Eclipsing binaries with excess luminosity from an accretion disk and/or hot spot (green) are to the upper left, including one system with an asymmetric light curve profile (light green) and four systems with a peak in the light curve that lags the secondary eclipse (orange). One system exhibits ellipsoidal modulation (brown) in a moderately eccentric orbit. The 22 eclipsing binaries exhibiting genuine reflection effects (blue) have nearly circular orbits and form a distinct population toward the bottom left with $\Theta_{\rm max} < 0.03$ and $\Delta I_2/\Delta I_1 < 0.4$ (blue solid lines). The three systems that may also show reflection effects (cyan) have slightly different properties and lie outside our adopted parameter space.

In addition to the selection effects discussed in §1, the difficulty in detecting low-mass eclipsing companions to B-type MS stars partially stems from the small number of nearby B-type MS stars in our Milky Way galaxy. Quantitatively, there are only ≈6,000 B-type stars with robust parallactic distances $d < 500$ pc (Perryman et al. 1997). This is a factor of ≈30 times smaller than the number of B-type MS stars $\mathcal{N}_{\rm B} \approx 174{,}000$ in our OGLE-III LMC sample. It is therefore not surprising that we have not yet observed in the Milky Way the precise counterparts to our reflecting eclipsing binaries with B-type MS primaries and low-mass pre-MS companions.

2.2.2. *Other Intriguing Light Curves*

We now discuss the remaining 16 unusual systems in our OGLE-III LMC sample. The properties of these 16 eclipsing binaries are not fully understood, and may potentially have important implications for the evolution of close binaries. However, they have distinctly different light curve parameters and physical characteristics than those in our 22 reflecting MS + pre-MS eclipsing binaries. A detailed study of these 16 unusual systems is therefore not in the scope of the present study. We only summarize the observed properties of these 16 systems to illustrate the uniqueness of our nascent eclipsing binaries.

The 12 eclipsing binaries in the top left of Fig. 3 have deep secondary eclipses and large out-of-eclipse variations that are not necessarily symmetric with respect to the eclipses. The lack of symmetry dictates that the variations cannot be solely due to reflection effects. Moreover, the deeper secondary eclipses in these systems indicate excess light from a hot spot and/or accretion disk. Similar systems exist in our Milky Way such as V11 in the old open cluster NGC 6791 (de Marchi et al. 2007), T-And0-00920 in the galactic field (Devor et al. 2008), and SRa01a_34263 in the young open cluster NGC 2264 (Klagyivik et al. 2013). Quantitatively, these 12 eclipsing binaries with luminous disks and/or hot spots have $\Delta I_2/\Delta I_1 > 0.4$, while our

Table 1. Analytic model parameters of 38 eclipsing binaries with intriguing light curves.

Catalog Properties			Analytic Model Parameters											
ID	$\langle V-I\rangle$	$\mathcal{N}_I$	P	t_o	$\langle I\rangle$	ΔI_1	Θ_1	Φ_2	ΔI_2	Θ_2	$\Delta I_{\rm refl}$	$\mathcal{N}_c$	$\chi^2_{\rm GS}/\nu$	Type
1500	0.17	440	6.025412	3563.908	17.883	1.023	0.0201	0.565	0.160	0.0240	0.035	1	1.29	Ellipsoidal
1675	0.04	465	8.697351	3568.781	17.277	0.310	0.0159	0.528	0.294	0.0136	0.037	1	1.21	Disk/Spot
1803	−0.07	460	3.970086	3572.117	17.090	0.637	0.0162	0.501	0.096	0.0156	0.138	1	1.55	Reflection
1965	−0.09	440	3.175248	3570.628	17.221	0.197	0.0219	0.497	0.073	0.0275	0.017	2	1.10	Reflection
2139	−0.16	477	8.462510	3576.045	16.507	0.328	0.0103	0.502	0.031	0.0089	0.033	2	1.28	Reflection
3972	0.06	448	3.396033	3565.053	17.882	0.263	0.0170	0.496	0.148	0.0199	0.023	2	4.14	Possible Reflection
5205	−0.04	456	4.164725	3564.819	16.682	0.162	0.0225	0.499	0.071	0.0221	0.044	1	1.22	Possible Reflection
5377	−0.11	447	3.276364	3563.150	17.346	0.165	0.0178	0.502	0.047	0.0202	0.020	1	1.18	Reflection
5776	−0.03	856	4.715550	3564.833	17.282	0.283	0.0166	0.514	0.174	0.0219	0.042	2	2.06	Disk/Spot (Asym.)
5898	−0.05	439	5.323879	3567.545	16.752	0.834	0.0212	0.501	0.141	0.0215	0.098	1	1.13	Reflection
6630	−0.02	410	3.105571	3563.821	17.104	0.164	0.0205	0.497	0.058	0.0210	0.019	1	1.16	Reflection
7419	0.13	421	4.255889	3563.579	16.502	0.185	0.0180	0.497	0.035	0.0135	0.037	2	1.11	Reflection
7842	−0.05	477	3.781798	3565.825	17.966	1.725	0.0148	0.498	0.181	0.0148	0.083	1	1.24	Reflection
9002	0.04	424	3.578291	3568.696	18.069	0.243	0.0156	0.490	0.137	0.0263	0.173	2	2.08	Disk/Spot (Lag)
9642	0.11	782	3.913360	3565.613	17.933	0.699	0.0174	0.502	0.064	0.0143	0.050	1	1.23	Reflection
10289	−0.09	557	4.642567	3566.031	16.833	0.199	0.0144	0.499	0.038	0.0148	0.034	1	1.09	Reflection
10941	−0.02	559	4.079727	3563.840	17.585	0.154	0.0211	0.401	0.064	0.0229	0.041	2	1.26	Disk/Spot (Lag)
11731	−0.04	477	5.661823	3544.866	16.837	0.059	0.0181	0.529	0.030	0.0169	0.065	1	1.65	Disk/Spot (Lag)
11787	−0.03	493	3.305829	3542.971	17.757	0.487	0.0202	0.500	0.401	0.0201	0.024	0	1.09	Disk/Spot
12528	0.03	476	8.187359	3537.820	17.749	0.240	0.0153	0.498	0.211	0.0153	0.019	2	1.15	Disk/Spot
13194	0.05	493	11.535650	3557.945	17.826	0.234	0.0079	0.498	0.262	0.0103	0.048	2	1.36	Disk/Spot (Lag)
13721	−0.10	428	3.122558	3558.192	17.818	0.420	0.0169	0.500	0.096	0.0185	0.025	1	1.01	Reflection
15306	−0.03	537	12.654262	3580.455	17.955	0.612	0.0068	0.501	0.430	0.0074	0.058	2	0.92	Disk/Spot
15761	−0.11	223	5.310911	3581.568	16.530	0.850	0.0147	0.504	0.101	0.0142	0.108	2	2.86	Reflection
15792	−0.11	600	4.317022	3566.098	16.721	0.231	0.0140	0.500	0.041	0.0156	0.039	2	1.63	Reflection
16828	−0.16	606	3.675697	3572.011	16.618	0.109	0.0174	0.502	0.032	0.0146	0.018	2	1.26	Reflection
17217	−0.12	592	5.354795	3576.802	16.543	0.098	0.0114	0.490	0.033	0.0096	0.022	2	1.24	Reflection
17387	−0.17	605	4.772926	3567.419	16.157	0.094	0.0219	0.499	0.026	0.0228	0.017	0	1.15	Reflection
17695	0.01	473	3.096068	3567.092	17.343	0.176	0.0208	0.501	0.148	0.0228	0.019	2	0.92	Disk/Spot
18330	−0.01	599	3.252913	3561.424	16.104	0.297	0.0253	0.502	0.073	0.0252	0.056	2	2.75	Reflection
18419	−0.13	599	4.118145	3564.319	16.741	0.545	0.0158	0.485	0.086	0.0175	0.059	2	1.83	Reflection
19186	0.01	473	5.652474	3567.458	17.701	0.278	0.0130	0.500	0.187	0.0150	0.019	1	0.94	Disk/Spot
21025	−0.10	435	4.543290	3581.225	16.777	0.134	0.0182	0.491	0.033	0.0138	0.025	1	0.97	Reflection
21452	0.17	377	8.178958	3541.898	17.362	2.824	0.0111	0.525	0.172	0.0098	0.124	2	1.86	Reflection
21641	0.05	436	3.092424	3572.506	16.741	0.405	0.0191	0.500	0.073	0.0191	0.062	1	0.76	Reflection
21859	0.00	428	3.154536	3571.735	16.172	0.617	0.0296	0.499	0.232	0.0332	0.080	1	1.23	Possible Reflection
21975	0.13	437	3.021139	3571.601	16.208	0.139	0.0196	0.500	0.029	0.0160	0.030	0	1.11	Reflection
23981	0.09	435	5.720508	3579.130	16.861	0.152	0.0215	0.499	0.144	0.0213	0.076	0	1.17	Disk/Spot

22 systems with low-luminosity pre-MS companions have $\Delta I_2/\Delta I_1 < 0.4$.

Our 22 eclipsing binaries with pre-MS companions have nearly circular orbits with $|\Phi_2 - 1/2| \leq 0.025$, as expected from tidal damping even earlier in their pre-MS phase of evolution (Zahn & Bouchet 1989). One peculiar eclipsing binary, ID-1500 (brown system in Fig. 3), satisfies our selection criteria of $\Theta_{\rm max} < 0.03$ and $\Delta I_2/\Delta I_1 < 0.4$, but has a moderately eccentric orbit of $e > e_{\rm min}(\Phi_2 = 0.565) = 0.10$ according to Eq. 2. This eclipsing binary has a deep primary eclipse $\Delta I_1 = 1.0$ mag that stipulates the binary components cannot both be normal MS stars. However, the light curve of ID-1500 peaks at $\phi \approx 0.8$, i.e. $\phi \approx -0.2$ as folded in Fig. 3, suggesting the out-of-eclipse variations are due to ellipsoidal modulations in an eccentric orbit instead of reflection effects. Specifically, periastron in this system probably occurs near $\phi \approx -0.2$, at which point the stars are tidally deformed into oblate ellipsoids and the perceived flux is increased. We attempt to fit a detailed physical model (see §3) to this system assuming the companion is a pre-MS star, but our fit is rather poor with $\chi^2/\nu = 1.7$. Moreover, our physical model converges toward an unrealistic solution with $q \approx 0.5$. Whether the out-of-eclipse variations in this system are due to reflection effects or are entirely because of ellipsoidal modulations, the removal of this one system does not affect our investigation of low-mass $q < 0.25$ companions to B-type MS stars.

We find three additional eclipsing binaries that may display reflection effects with a pre-MS companion, but lie just outside of our selected parameter space (cyan systems in Fig. 3). ID-21859 has a broad eclipse $\Theta_{\rm max} = 0.033$, but has eclipse depth properties that separate it from the observed Algol population. ID-3972 and ID-5205 have slightly deeper secondary eclipses $\Delta I_2/\Delta I_1 \approx 0.5$, but exhibit symmetric light curve profiles with no immediate indications of disks and/or hot spots. In our Monte Carlo simulations (§5), we implement the same selection criteria utilized here, and so we do not include these three systems in our statistical sample. Moreover, the observed population of eclipsing binaries with genuine reflection effects are concentrated near $\Theta_{\rm max} \approx 0.018$ and $\Delta I_2/\Delta I_1 \approx 0.2$. Increasing distance from this center according to our adopted metric increases the likelihood that the system is not a MS + pre-MS eclipsing binary. Our 22 eclipsing binaries that exhibit pronounced reflection effects $\Delta I_{\rm refl} > 0.015$ mag with pre-MS companions at $P = 3.0$-8.5 days have $\Theta_{\rm max} \leq 0.03$, which cleanly differentiates them from Algols and contact binaries that fill their Roche lobes, $\Delta I_2/\Delta I_1 \leq 0.4$, which distinguishes

them from systems with luminous disks and/or hot spots, and $|\Phi_2 - {}^1/_2| \leq 0.025$, which separates them from systems that show ellipsoidal modulations in an eccentric orbit (Fig. 3). We emphasize that these criteria are rather effective in selecting systems with low-mass pre-MS companions while simultaneously minimizing contamination from other types of eclipsing binaries.

2.3. *Comparison to Previously Known Classes*

2.3.1. *Irradiated Binaries*

Other classes of detached binaries can exhibit intense irradiation effects, but there are key differences that distinguish our 22 systems. Namely, our 22 eclipsing binaries contain a hot MS primary with a cool pre-MS companion, while most previously known reflecting eclipsing binaries contain a hot evolved remnant with a cool MS companion (Bond 2000; Lee et al. 2009). For example, eclipsing binaries with subdwarf B-type (sdB) primaries and M-dwarf companions, sometimes called HW Vir eclipsing binaries after the prototype, have similar reflection effect amplitudes and light curve properties (Lee et al. 2009; Barlow et al. 2013; Pietrukowicz et al. 2013). However, HW Vir systems differ from our systems in three fundamental parameters. First, the sdB primaries in HW Vir eclipsing binaries are intrinsically ∼100 times less luminous than B-type MS stars, and would therefore not be detectable in the LMC given the sensitivity of the OGLE-III survey. Second, HW Vir eclipsing binaries have shorter orbital periods $P \lesssim 0.5$ days than our 22 systems with $P = 3.0$ - 8.5 days. This is because the sdB primaries and M-type MS secondaries are smaller and less luminous than our B-type MS primaries and pre-MS companions, and therefore must be closer together to produce observable reflection effects. Finally, HW Vir systems are evolved binaries and associated with old stellar populations, while our 22 nascent eclipsing binaries are situated in or near star-forming H II regions (see §4).

As another example, binaries in which a MS star orbits the hot central star of a planetary nebula can pass through a very brief interval $\lesssim$10,000 yrs when reflection effects are detectable, although eclipses are generally not observed (Bond 2000). Such systems could have satisfied our magnitude and color criteria, but these binaries are typically at shorter periods $P < 3$ days than we have selected (Miszalski et al. 2009). Moreover, we cross-referenced the positions of our 22 systems with catalogs of planetary nebulae (Reid & Parker 2010) and emission-line point sources (Howarth 2013) in the LMC, and do not find any matches. Our nascent B-type MS + pre-MS eclipsing binaries clearly exhibit a phenomenologically different type of reflection effect than those observed in evolved binaries with stellar remnants.

2.3.2. *Pre-MS Binaries*

Although there is a rich literature regarding pre-MS binaries (see Hillenbrand & White 2004 and review by Mathieu 1994), only a few close MS + pre-MS binaries have been identified. For example, photometric and spectroscopic observations of the eclipsing binaries EK Cep (Popper 1987), AR Aur (Nordstrom & Johansen 1994), TY CrA (Casey et al. 1998), and RS Cha (Alecian et al. 2007) have demonstrated the primaries are close to the zero-age MS while the secondaries are still contracting on the pre-MS. However, these systems have late-B/A-type MS primaries ($M_1 \approx 1.9$ - $3.2\,M_\odot$), components of comparable mass ($q \approx 0.5$ - 1.0), and temperature contrasts ($T_2/T_1 \approx 0.4$ - 0.9) that are too small to produce detectable reflection effects. Morales-Calderón et al. (2012) identified ISOY J0535-447 as a young pre-MS eclipsing binary with an extreme mass ratio $q \approx 0.06$, but with a low-mass $M_1 \approx 0.8\,M_\odot$ early-K primary.

The only similar analog of a B-type MS primary with a closely orbiting low-mass pre-MS companion is the eclipsing binary BM Orionis (Hall & Garrison 1969; Palla & Stahler 2001; Windemuth et al. 2013), although the nature of its secondary has been debated and has even been suggested to be a black hole (Wilson 1972). Located in the heart of the Orion Nebula, BM Ori exhibits broad eclipses with noticeable undulations in the eclipse shoulders. These features indicate the companion nearly fills its Roche lobe and is still accreting from the surrounding disk. If BM Ori contains an accreting pre-MS companion, then it could be a precursor to our 22 eclipsing binaries that show no evidence for an accretion disk. Indeed, BM Ori is extremely young with an age $\tau \lesssim 0.1$ Myr estimated from pre-MS contraction timescales (Palla & Stahler 2001) and the dynamics of the inner region of the Orion Nebula (O'Dell et al. 2009). Meanwhile, the disk photoevaporation timescale around Herbig Be pre-MS stars with $M_1 \approx 3$ - $8\,M_\odot$ is ≈0.3 Myr (Alonso-Albi et al. 2009). It is therefore not unexpected that BM Ori at $\tau < 0.1$ Myr still has a disk. Alternatively, our 22 systems no longer have a noticeable accretion disk in the photometric light curves, and so must be older than $\tau \gtrsim 0.3$ Myr (see also §3.3).

If BM Ori was placed in the LMC and observed by the OGLE-III survey, it would not be contained in our sample for three reasons. First, BM Ori contains an extremely young and reddened mid-B MS primary with $M_1 \approx 6\,M_\odot$, $\langle V - I \rangle \approx 0.8$, and $\langle I \rangle \approx 8.8$ at the distance $d \approx 400$ pc to the Orion Nebula (Windemuth et al. 2013). It would be rather faint at $\langle I \rangle \approx 19.3$ if located at the distance $d = 50$ kpc to the LMC, and therefore below our photometric selection limit. Second, even if we extended our search toward fainter systems, the reflection effect amplitude in BM Ori is too small to be observed given the sensitivity of the OGLE-III LMC observations. Finally, the secondary eclipse is extremely shallow with undulations in the eclipse shoulders. We could not measure well-defined secondary eclipse parameters according to our analytic model. In addition to being at a fundamentally different stage of evolution, i.e. still accreting from a disk, BM Ori has clearly different photometric light curve properties than those of our 22 eclipsing binaries.

Finally, BM Ori has a modest mass ratio $q = 0.31$. In contrast, the majority of our reflecting eclipsing binaries have extreme mass ratios $q < 0.25$ (see below), as indicated by their more luminous, massive primaries and larger reflection effect amplitudes. Our reflecting eclipsing binaries represent the first detection of B-type MS stars with close extreme mass-ratio companions where the orbital periods and the nature of the companions are reliably known.

3. PHYSICAL PROPERTIES

3.1. *Overview of Methodology*

The component masses in eclipsing binaries are typically measured dynamically via spectral radial velocity variations. However, our eclipsing binaries in the LMC are relatively faint $16 < \langle I \rangle < 18$ and typically embedded in H II regions (§4) that would contaminate the stellar spectra with nebular emission lines. Moreover, B-type MS stars experience slight atmospheric variations and rotate so rapidly that their spectral absorption lines are generally broadened by $v_{\rm surface} \approx 100$ - 250 km s^{-1} (Abt et al. 2002; Levato & Grosso 2013). There is a small population of slowly rotating B-type MS stars with $v_{\rm surface} \approx 50$ km s^{-1}, and Abt et al. (2002) and Levato & Grosso (2013) suggest these systems may by tidally synchronized with closely orbiting low-mass companions. Indeed, our reflecting eclipsing binaries may partially explain the origins of B-type MS slow rotators. In any case, it would be quite observationally expensive to detect small velocity semi-amplitudes $K_1 \approx 25\,(q/0.1)$ km s^{-1} induced by closely orbiting low-mass companions for all 22 eclipsing binaries in our statistical sample. In the future, we plan to obtain multi-epoch spectra for a small subset of our MS + pre-MS eclipsing binaries. To analyze all 22 systems, however, we must currently utilize a different technique of inferring the physical properties based solely on the observed photometric light curves.

Fortunately, we have two additional constraints that allow us to estimate the masses of the binary components from the observed eclipse properties. First, our eclipsing binaries are detached from their Roche lobes, as demonstrated by their narrow eclipses, and therefore the primary and secondary are each effectively evolving along their respective single-star sequences (see §3.4 for further justification of this expectation and a discussion of systematic uncertainties). Given an age τ and masses M_1 and M_2, we can interpolate stellar radii R_1 and R_2, photospheric temperatures T_1 and T_2, and luminosities L_1 and L_2 from theoretical stellar evolutionary tracks. We can then use empirical bolometric corrections and color indices to map the physical properties of the eclipsing binaries into observed magnitudes and colors. Devor & Charbonneau (2006) and Devor et al. (2008) employed a similar technique of estimating ages and masses of galactic eclipsing binaries by incorporating stellar isochrones into their photometric light curve modeling. Their algorithm worked for a small subset of systems. In general, however, the parameters τ, M_1, and M_2 were generally degenerate, not unique, and/or not constrained.

This brings us to our second constraint. Unlike the sample of galactic eclipsing binaries studied by Devor et al. (2008), we know the distances to our 22 eclipsing binaries in the LMC. This extra distance constraint fully eliminates the degeneracy and allows us to calculate unique solutions for the physical properties of the eclipsing binaries. The deductions of the physical parameters progress as follows. The measured mean magnitude $\langle I \rangle$ and color $\langle V-I \rangle$, along with the distance, bolometric corrections, and color indices, mainly provide the luminosity L_1 of the B-type MS primary and the amount of dust reddening $E(V-I)$, respectively. From MS stellar evolutionary tracks, we can estimate the mass M_1 and radius R_1 of a young B-type MS star with luminosity L_1. The amplitude of the reflection effect $\Delta I_{\rm refl}$ is an indicator of T_2/T_1 and R_2/R_1 as discussed in §2, but also depends on the albedo of the secondary A_2. The sum of eclipse widths $\Theta_1 + \Theta_2$ determines the sum of the relative radii $(R_1 + R_2)/a$, the ratio of eclipse depths $\Delta I_2/\Delta I_1$ gives the luminosity contrast L_2/L_1, and the magnitude of the primary eclipse depth ΔI_1 provides the inclination i. Since we already know M_1, R_1 and L_1, we can infer R_2 and L_2 directly from the observed light curve parameters. Finally, according to pre-MS evolutionary tracks, the radius R_2 and luminosity L_2 of the pre-MS secondary uniquely corresponds to its age τ and mass M_2. In our full procedure (see below), we calculate each of these parameters simultaneously in a self-consistent manner. We also consider various sources of systematic errors in our measured light curve parameters as well as stellar evolutionary tracks. Nonetheless, the steps discussed above illustrate how we can estimate the physical properties of detached, unevolved, eclipsing binaries with known distances using only the photometric light curves.

3.2. *Physical Model Fits*

In our eclipsing binary models, we have eight physical parameters: orbital period P, epoch of primary eclipse minimum $t_{\rm o}$, primary mass M_1, secondary mass M_2, age τ, inclination i, albedo of the secondary A_2, and amount of dust extinction A_I toward the system. B-type MS stars in the LMC have slightly subsolar metallicities $\log(Z/{\rm Z}_\odot) \approx -0.4$ (Korn et al. 2000), where ${\rm Z}_\odot \approx 0.015$. We therefore incorporate the Padova Z=0.008, Y=0.26 stellar evolutionary tracks to describe the MS evolution (Bertelli et al. 2009), and the Pisa Z=0.008, Y=0.265, $\alpha = 1.68$, $X_D = 2\times10^{-5}$ tracks to model the pre-MS evolution (Tognelli et al. 2011). The physical properties of the binary components, e.g. radii R_1 and R_2, surface temperatures T_1 and T_2, luminosities L_1 and L_2, and surface gravities g_1 and g_2, are then interpolated from these stellar tracks according to the model parameters M_1, M_2, and τ. We use updated, temperature-dependent color indices and bolometric corrections (Pecaut & Mamajek 2013) to transform the intrinsic luminosities and temperatures of both binary components into combined absolute magnitudes M_I and M_V. We adopt the dust reddening law of $E(V-I) = 0.7A_I$ (Cardelli et al. 1989; Fitzpatrick 1999; Ngeow & Kanbur 2005) and LMC distance modulus of $\mu = 18.5$ (Pietrzyński et al. 2013) to then calculate the observed magnitudes $\langle I \rangle = M_I + \mu + A_I$ and $\langle V \rangle = M_V + \mu + 1.7A_I$.

We primarily utilize the eclipsing binary modeling software NIGHTFALL[2] to synthesize I-band and V-band light curves. We implement a square-root limb darkening law with the default limb-darkening coefficients, the default gravity brightening coefficients, model atmospheres according to the surface gravities of the binary components, fractional visibility of surface elements, three iterations of reflection effects, and the default albedo of $A_1 = 1.0$ for the hot B-type MS primaries.

[2] http://www.hs.uni-hamburg.de/DE/Ins/Per/Wichmann/Nightfall.html

Given the sensitivity of the OGLE-III data, the 19 eclipsing binaries with $|\Phi_2 - 1/2| < 0.01$ and $\Theta_1 \approx \Theta_2$ have $e < 0.02$ (see Eqn. 2 and Kallrath & Milone 2009). For these 19 systems, we assume circular orbits in our physical models. The three systems (ID-17217, ID-18419, and ID-21452) in slightly eccentric orbits with $0.010 \leq |\Phi_2 - 1/2| \leq 0.025$ have longer orbital periods where tidal effects are not as significant. The eclipse widths $\Theta_1 \approx \Theta_2$ are also comparable to each other in these three eclipsing binaries, dictating the eccentricities $0.02 < e < 0.08$ are small. Because the orbits are so close to circular, we cannot easily break the degeneracy between the eccentricity e and the argument of periastron ω. For these three systems, we impose $e = e_{\rm min}/\langle\cos(\omega)\rangle = 1.6\,e_{\rm min}$ according to Eqn. 2, where we have assumed a uniform probability distribution for ω. Adjusting the eccentricities to values within $e_{\rm min} < e < 2.2e_{\rm min}$ do not change the fitted model parameters beyond the uncertainties. For ID-21452, which has $\Phi_2 > 0.5$, we assume $\omega = 50^{\rm o}$. For ID-17217 and ID-18419, which have $\phi_2 < 0.5$, we adopt $\omega = 230^{\rm o}$. Changing the argument of periastron to the opposite angle, e.g. $\omega = 310^{\rm o}$ for ID-21452 or $\omega = 130^{\rm o}$ for ID-17217 and ID-18419, has a negligible effect on the other model parameters considering the eccentricities are so small.

Since tides have fully or nearly circularized the orbits, the rotation rates of the pre-MS companions with large convective envelopes are expected to be tidally synchronized with the orbital periods (Zahn & Bouchet 1989). For example, a $1.5\,{\rm M}_\odot$ pre-MS star with age $\tau = 1$ Myr in a $P = 4$ day orbit with a $10\,{\rm M}_\odot$ B-type MS star has rapid synchronization and spin-orbit alignment timescales of $\lesssim$0.01 Myr (Hut 1981; Belczynski et al. 2008). Meanwhile, the circularization timescale is orders of magnitude longer at $\approx$2 Myr, which is still only a small fraction of the secondary's pre-MS lifetime of $\approx$10 Myr. Hence, it is not surprising that all of our eclipsing binaries with $P < 4$ days have been circularized, while three systems with $P > 4$ days are in slightly eccentric orbits with $e \approx 0.03$ - 0.06.

B-type MS stars have radiative envelopes, and so tidal damping is not as efficient. Although the B-type MS primaries may spin independently from the orbital periods, we assume for simplicity that they are also tidally locked with the orbit (see also discussion of B-type MS slow rotators in §3.1). B-type MS stars become oblate only if they rotate close to their break-up speed or nearly fill their Roche lobes (Ekström et al. 2008b). Fortunately, young B-type MS stars typically rotate more slowly than their break-up speed (Abt et al. 2002; Ekström et al. 2008b; Levato & Grosso 2013), and the B-type MS primaries in our eclipsing binaries are well-detached from their Roche lobes. Even if the B-type MS primaries are not already synchronized with the orbit, their true shapes will differ only slightly from our model assumptions. For example, a B-type MS primary that quickly spins at $v_{\rm surface} = 300$ km s^{-1} will have an equatorial radius that is only 6% larger than its polar radius (Ekström et al. 2008b).

We show in Fig. 4 the reflection effect amplitude $\Delta I_{\rm refl}$ for three secondary masses $M_2 = 1$, 2, and 3 $M_\odot$ based on our NIGHTFALL models and adopted evolutionary tracks. For these sequences, we fix the other parameters at representative values of $M_1 = 10\,{\rm M}_\odot$, $P = 4$ days, $i = 90^{\rm o}$, and $A_2 = 0.7$. The observable pre-MS duration of the $3\,{\rm M}_\odot$ companion is only $\sim$2% the MS lifetime of the primary. Hence, the majority of our eclipsing binaries that display reflection effects must have $q < 0.3$ because the likelihood of observing a pre-MS + MS binary at larger q is very low. The radii of MS companions with $q < 0.15$ are too small to produce detectable eclipses given the cadence and sensitivity of the OGLE-III observations. We can therefore observe extreme mass-ratio eclipsing binaries only when the companion is large and still contracting on the pre-MS.

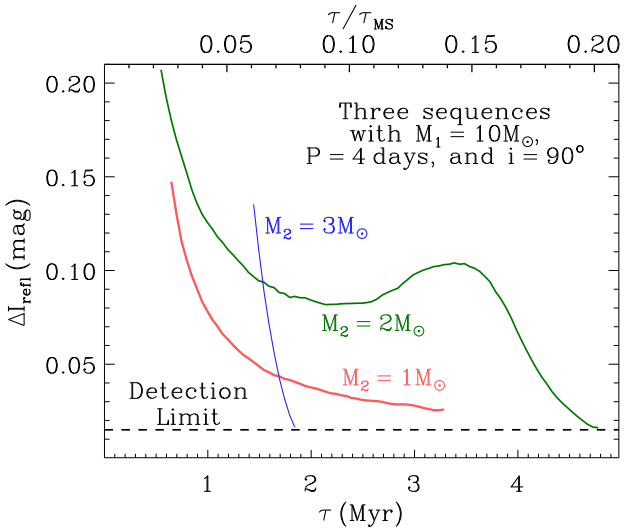

FIG. 4.— Reflection effect amplitude $\Delta I_{\rm refl}$ as a function of age τ for three secondary masses M_2. Above is time in units of the MS lifetime $\tau_{\rm MS} = 24$ Myr of the *primary* B-type MS star. We show only the portions of the evolution where the light curve properties satisfy our selection criteria. At early times $\tau \lesssim (0.02$ - $0.06)\,\tau_{\rm MS}$, the companions have Roche-lobe fill-factors $RLF_2 \gtrsim 80\%$ and are difficult to distinguish from large, evolved subgiants. At later times $\tau \gtrsim (0.1$ - $0.2)\,\tau_{\rm MS}$, the secondary becomes substantially smaller as it approaches its own MS phase of evolution. Not only do the reflection effects fall below the detection limit of $\Delta I_{\rm refl} = 0.015$ mag (dashed line), but the eclipse depths can also diminish below the sensitivity of the OGLE-III LMC observations. Extreme mass-ratio binaries $q \lesssim 0.15$ (red) produce observable eclipses only when the companions are on the early pre-MS phase of evolution. Binaries at moderate mass ratios $q \gtrsim 0.3$ (blue) spend only $\lesssim$2% of the primary's evolution in such a MS + pre-MS combination. The nonmonotonic behavior in $\Delta I_{\rm refl}$ for the $M_2 = 2{\rm M}_\odot$ sequence (green) is due to the complex pre-MS evolution of stars with $M > 1.4{\rm M}_\odot$, which undergo different processes of nuclear fusion and energy transport.

The correction factor $f_\sigma(I)$ for the photometric errors we calculated in §2.1 can differ between systems, even if they have the same magnitude. We therefore do not use the simple relation in Eq. 5 in our physical models. Instead, we calculate the correction factors between the catalog photometric errors and intrinsic rms scatter for each of our 22 eclipsing binaries individually. To achieve this, we separately fit 3$^{\rm rd}$ degree polynomials across the out-of-eclipse intervals $0.05 < \phi < 0.45$ and $0.55 < \phi < 0.95$ for each of the I-band and V-band light curves. We remove all residuals that exceed 4σ, measure the rms dispersions of the remaining residuals, and then calculate the correction factors $f_{\sigma,I}$ and $f_{\sigma,V}$ between the catalog photometric errors and the measured rms scatter. For some light curves, there are too few data points to accurately measure the correction factors, so

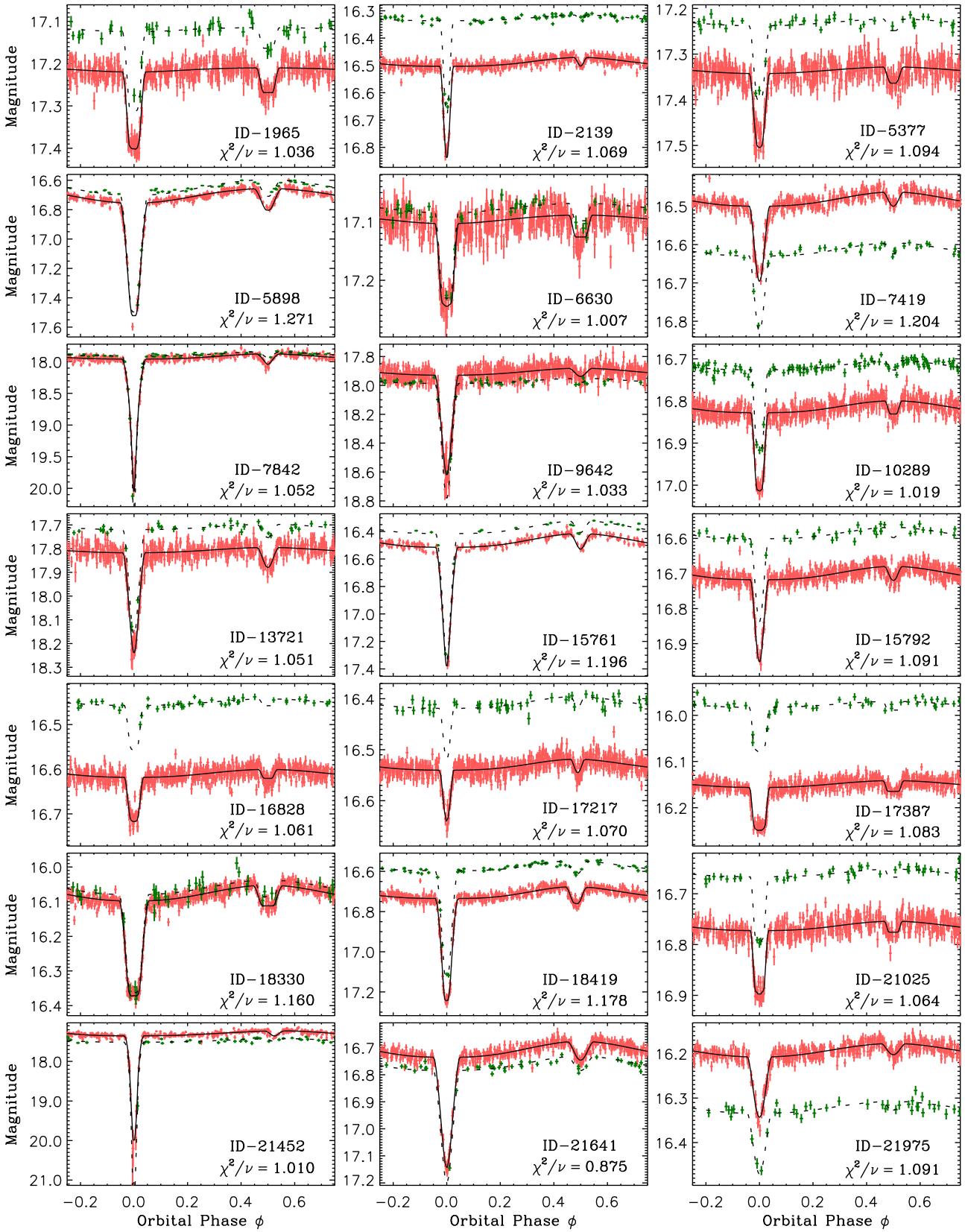

FIG. 5.— As shown in Fig. 1 for the prototype ID-1803, we compare the physical model fits to the the observed light curves for the remaining 21 eclipsing binaries with B-type MS primaries and irradiated pre-MS companions. We present the physical fit parameters and statistics for all 22 systems in Tables 2-3.

Table 2. Best-fit model parameters and statistics for 22 eclipsing binaries with reflection effects. The uncertainties reported in parenthesis, which include systematic uncertainties, are not necessarily symmetric around the best-fit model values.

	Physical Model Properties								Fit Statistics							
ID	P (days)	t_o (JD-2450000)	M_1 ($M_\odot$)	M_2 ($M_\odot$)	τ (Myr)	i (°)	A_2 (%)	A_I (mag)	$\mathcal{N}_I$	$\mathcal{N}_{c,I}$	$f_{\sigma,I}$	$\mathcal{N}_V$	$\mathcal{N}_{c,V}$	$f_{\sigma,V}$	χ^2/ν	PTE
1803	3.970085 (7)	3572.1174 (9)	10.4 (1.6)	0.8 (0.2)	0.7 (0.4)	83.6 (1.1)	97 (17)	0.32 (4)	460	1	1.17	41	0	1.21	1.062	0.167
1965	3.175265 (9)	3570.6285 (17)	7.7 (1.2)	1.9 (0.3)	15 (4)	89.8 (1.5)	100 (28)	0.22 (3)	440	2	1.09	45	0	1.50	1.036	0.283
2139	8.462504 (21)	3576.0465 (23)	12.7 (2.0)	1.9 (0.4)	0.9 (0.5)	84.0 (1.3)	29 (15)	0.23 (3)	477	2	1.19	70	1	1.16	1.069	0.132
5377	3.276373 (10)	3563.1493 (19)	7.4 (1.2)	1.2 (0.2)	14 (5)	84.8 (1.6)	68 (22)	0.19 (3)	447	1	1.11	43	0	1.08	1.094	0.075
5898	5.323855 (13)	3567.5433 (17)	7.7 (1.5)	3.8 (0.8)	0.8 (0.4)	83.5 (1.5)	86 (25)	0.07 (3)	439	1	1.30	44	2	1.25	1.271	<0.001
6630	3.105556 (9)	3563.8238 (16)	8.3 (1.3)	1.5 (0.2)	13 (4)	86.5 (1.3)	100 (27)	0.34 (4)	410	1	1.12	40	0	1.05	1.007	0.450
7419	4.255885 (9)	3563.5793 (14)	13.7 (2.4)	1.7 (0.3)	5.2 (1.5)	81.1 (2.1)	61 (21)	0.66 (7)	421	2	1.12	40	0	1.10	1.204	0.002
7842	3.781792 (8)	3565.8256 (10)	6.0 (0.9)	2.0 (0.3)	2.6 (0.8)	88.5 (0.8)	60 (16)	0.17 (3)	477	1	1.13	72	0	1.08	1.052	0.197
9642	3.913363 (9)	3565.6120 (14)	6.4 (1.0)	2.3 (0.4)	1.7 (0.5)	81.2 (1.4)	29 (19)	0.29 (4)	782	1	1.16	40	1	1.05	1.033	0.249
10289	4.642579 (11)	3566.0280 (15)	11.2 (1.8)	0.8 (0.2)	2.5 (0.7)	86.9 (0.9)	100 (18)	0.32 (4)	557	1	1.07	115	0	1.05	1.019	0.357
13721	3.122554 (11)	3558.1903 (16)	6.2 (1.0)	1.5 (0.3)	8 (2)	83.3 (2.0)	37 (16)	0.14 (3)	428	1	1.05	40	0	1.05	1.051	0.214
15761	5.310910 (12)	3581.5694 (14)	12.6 (2.4)	2.3 (0.4)	1.9 (0.5)	85.4 (1.1)	78 (17)	0.30 (4)	223	0	1.74	21	0	1.37	1.196	0.021
15792	4.317015 (9)	3566.0986 (15)	11.5 (1.8)	1.6 (0.3)	2.8 (1.0)	83.3 (1.7)	69 (22)	0.30 (4)	600	1	1.35	40	0	1.41	1.091	0.056
16828	3.675702 (10)	3572.0106 (17)	10.8 (1.7)	1.0 (0.2)	7 (2)	83.7 (2.0)	100 (23)	0.23 (3)	606	3	1.18	47	0	1.05	1.061	0.137
17217[a]	5.354787 (20)	3576.8028 (26)	11.3 (1.8)	1.7 (0.4)	7 (3)	81.6 (2.1)	100 (31)	0.28 (5)	592	3	1.18	47	0	1.37	1.070	0.109
17387	4.772901 (14)	3567.4122 (24)	12.4 (2.0)	1.2 (0.2)	8 (2)	89.6 (1.5)	100 (22)	0.23 (4)	605	1	1.17	47	1	1.34	1.083	0.071
18330	3.252921 (8)	3561.4274 (17)	14.6 (2.5)	1.6 (0.3)	5.6 (1.5)	89.5 (1.6)	100 (19)	0.46 (6)	599	2	1.48	46	0	3.04	1.160	0.003
18419[b]	4.118151 (8)	3564.3203 (12)	11.6 (2.0)	1.5 (0.3)	1.6 (0.5)	88.0 (1.1)	78 (17)	0.27 (4)	599	1	1.28	70	0	1.18	1.178	0.001
21025	4.543312 (13)	3581.2269 (22)	10.7 (1.7)	1.0 (0.3)	6 (2)	88.5 (1.6)	100 (26)	0.31 (4)	435	1	1.05	45	0	1.05	1.064	0.165
21452[c]	8.178961 (19)	3541.8978 (22)	10.1 (1.6)	2.4 (0.7)	0.6 (0.4)	89.3 (2.2)	67 (17)	0.61 (7)	337	1	1.43	40	0	1.88	1.010	0.436
21641	3.092426 (7)	3572.5059 (18)	12.7 (2.0)	1.9 (0.3)	2.6 (1.0)	82.8 (1.6)	51 (19)	0.54 (6)	436	1	1.05	45	0	1.05	0.875	0.976
21975	3.021141 (9)	3571.6002 (19)	16.0 (2.6)	1.7 (0.3)	4.0 (1.4)	77.9 (2.3)	36 (21)	0.68 (8)	437	1	1.16	42	0	1.72	1.091	0.084

(a): modeled with $e = 0.03$ and $\omega = 230^o$; (b): $e = 0.04$ and $\omega = 230^o$; (c): $e = 0.06$ and $\omega = 50^o$; the other 19 systems have circular orbits.

Table 3. Dependent physical properties derived by using main model parameters in Table 2 in combination with Kepler's laws and stellar evolutionary tracks. The representative uncertainties are 15% or 0.03, which ever is larger, in the mass ratios q and relative ages τ/τ_{MS}, 10% in orbital separation a, radii R_1 and R_2, and Roche-lobe fill factors $RLFF_1$ and $RLFF_2$, 8% in temperatures T_1 and T_2, 40% in luminosities L_1 and L_2, and 0.1 mag in absolute magnitudes M_I and M_V.

ID	q	τ/τ_{MS}	a ($R_\odot$)	R_1 ($R_\odot$)	R_2 ($R_\odot$)	$RLFF_1$	$RLFF_2$	T_1 (K)	T_2 (K)	L_1 ($L_\odot$)	L_2 ($L_\odot$)	M_I	M_V
1803	0.07	0.03	23	3.6	3.1	0.27	0.77	27,000	4,400	6,000	3	−1.7	−2.1
1965	0.24	0.35	19	3.6	1.4	0.39	0.29	23,000	9,900	3,000	17	−1.5	−1.7
2139	0.15	0.05	43	4.2	3.7	0.19	0.39	29,000	5,200	12,000	9	−2.2	−2.5
5377	0.16	0.33	19	3.5	1.2	0.36	0.30	22,000	6,100	3,000	2.2	−1.3	−1.6
5898	0.49	0.02	29	3.0	6.3	0.25	0.73	24,000	8,400	2,500	180	−1.8	−1.9
6630	0.18	0.41	19	3.9	1.3	0.41	0.31	23,000	7,800	4,000	6	−1.7	−2.0
7419	0.12	0.35	28	5.1	2.6	0.35	0.47	30,000	6,200	18,000	9	−2.7	−3.0
7842	0.33	0.04	20	2.7	2.9	0.29	0.53	21,000	5,700	1,200	8	−0.7	−0.9
9642	0.36	0.03	21	2.7	3.7	0.29	0.63	21,000	5,800	1,400	14	−0.9	−1.0
10289	0.07	0.13	27	4.0	1.5	0.26	0.34	28,000	4,300	9,000	0.7	−2.0	−2.3
13721	0.25	0.13	18	2.8	2.0	0.34	0.46	20,000	7,200	1,300	10	−0.8	−1.0
15761	0.18	0.12	32	4.3	4.0	0.27	0.56	29,000	6,100	12,000	20	−2.3	−2.6
15792	0.14	0.15	26	4.1	2.1	0.30	0.38	28,000	5,200	9,000	3	−2.1	−2.4
16828	0.09	0.33	23	4.4	1.2	0.34	0.30	27,000	4,500	9,000	0.6	−2.1	−2.4
17217	0.15	0.34	30	4.5	2.1	0.29	0.33	27,000	7,800	10,000	15	−2.2	−2.5
17387	0.09	0.48	28	5.2	1.4	0.33	0.26	28,000	5,300	15,000	1.4	−2.6	−2.9
18330	0.11	0.42	23	5.5	2.5	0.43	0.54	30,000	6,200	23,000	8	−2.9	−3.2
18419	0.13	0.08	25	4.0	2.4	0.31	0.48	28,000	5,000	9,000	3	−2.0	−2.4
21025	0.09	0.28	26	4.2	1.3	0.29	0.27	27,000	4,600	8,000	0.7	−2.0	−2.4
21452	0.24	0.02	40	3.6	5.2	0.20	0.58	27,000	5,200	6,000	17	−1.8	−2.0
21641	0.15	0.16	22	4.4	2.7	0.39	0.58	29,000	5,600	13,000	6	−2.3	−2.6
21975	0.11	0.34	23	5.5	2.5	0.44	0.56	32,000	5,800	28,000	6	−3.0	−3.3

we impose a minimum value of 1.05 for $f_{\sigma,I}$ and $f_{\sigma,V}$. For each of our 22 eclipsing binaries, we multiply the catalog photometric errors by their respective correction factors $f_{\sigma,I}$ and $f_{\sigma,V}$ when we fit our physical models.

To constrain the eight parameters in our physical models, we fit NIGHTFALL synthetic light curves to the I-band and V-band data simultaneously. As in §2, we use a Levenberg-Marquardt method to minimize the χ^2 statistic between the light curves and physical models. We clip up to $\mathcal{N}_{c,I} + \mathcal{N}_{c,V} \leq 3$ data points that deviate more than 4σ from our best-fit model. Since we fit both the I-band and V-band together, there are $\nu = \mathcal{N}_I + \mathcal{N}_V - \mathcal{N}_{c,I} - \mathcal{N}_{c,V} - 8$ degrees of freedom. We compare the observed light curves to our best physical model fits in Fig. 1 (for our prototype ID-1803) and Fig. 5 (for the remaining 21 reflecting eclipsing binaries). We present the fit parameters and statistics in Table 2, and other physical properties in Table 3.

3.3. *Results*

For 21 of our 22 eclipsing binaries, our models have good fit statistics $\chi^2/\nu = 0.87$ - 1.20. The one remaining eclipsing binary, ID-5898, has a poor fit with $\chi^2/\nu = 1.27$, i.e. a probability to exceed χ^2

of $PTE < 0.001$, most likely caused by third light contamination. We discuss third light contamination and other systematic uncertainties in §3.4.

For the 21 eclipsing binaries with good fit statistics, we measure primary masses $M_1 = 6\text{-}16\,M_\odot$ appropriate for early B-type MS stars, low-mass secondaries $M_2 = 0.8\text{-}2.4\,M_\odot$ ($q = 0.07\text{-}0.36$), young ages $\tau = 0.6\text{-}15$ Myr, nearly edge-on inclinations $i = 78^o\text{-}90^o$, secondary albedos $A_2 = (30\text{-}100)\%$, and moderate to large dust extinctions $A_I = 0.14\text{-}0.68$ mag. The B-type MS primaries have relative ages $\tau/\tau_{\rm MS}$ that span from 2% up to 50% their MS lifetimes. The fits confirm these eclipsing binaries with narrow eclipses are in detached configurations with Roche-lobe fill-factors $RLFF_1 = 0.2\text{-}0.4$ and $RLFF_2 = 0.3\text{-}0.8$. Given the orbital separations $a = 20\text{-}40\,R_\odot$, these fill-factors correspond to physical radii $R_1 = 2.7\text{-}5.5\,R_\odot$ and $R_2 = 1.2\text{-}5.2\,R_\odot$. Finally, as expected for eclipsing binaries that exhibit substantial reflection effects, we find comparable radii $R_2/R_1 = 0.3\text{-}1.4$ but extreme contrasts in temperature $T_2/T_1 = 0.15\text{-}0.43$ and luminosity $L_2/L_1 \approx 10^{-4}\text{-}10^{-2}$.

Considering B-type MS stars span a narrow range of temperatures T_1 and radii R_1, the temperatures T_2 and radii R_2 of the companions are more accurately and robustly measured than their masses M_2 or ages τ. In Fig. 6, we compare the locations of the pre-MS companions on a Hertzsprung-Russell diagram to the theoretical Pisa evolutionary tracks (Tognelli et al. 2011). ID-5898 is biased toward larger L_2 most likely due to third light contamination (see below). ID-1965, ID-5377, and ID-6630 have small reflection effect amplitudes $\Delta I_{\rm refl} = 0.017\text{-}0.20$ mag just above our detection limit of 0.015 mag (see Fig. 5 and Table 1). These three systems also have shallow, flat-bottomed eclipses $\Delta I_1 \approx 0.2$ mag that dictate full non-grazing eclipse trajectories and ratio of radii $R_2/R_1 \approx 0.3\text{-}0.4$. The companions in these three eclipsing binaries are therefore small, warm, late pre-MS or zero-age MS stars with relatively older ages $\tau \approx 13\text{-}15$ Myr (Table 2). Nonetheless, these three systems still have small secondary masses $M_2 = 1.2\text{-}1.9\,M_\odot$ ($q = 0.16\text{-}0.24$), so we keep these eclipsing binaries in our statistical sample.

The remaining 18 systems have deeper eclipses and/or larger reflection effect amplitudes, which dictate the companions are larger and/or cooler. The secondaries in these 18 eclipsing binaries are inconsistent with zero-age MS stars (Fig. 6), but instead must be primordial pre-MS stars with young ages $\tau = 0.6\text{-}8$ Myr and small masses $M_2 = 0.8\text{-}2.4\,M_\odot$. The majority of these companions have developed a radiative core and are evolving with nearly constant R_2 on the Henyey track (Siess et al. 2000; Tognelli et al. 2011). A few secondaries are still fully convective and contracting on the Hyashi phase of the pre-MS. According to our adopted pre-MS evolutionary tracks (Tognelli et al. 2011), eleven of our pre-MS secondaries have not yet initiated stable nuclear burning in their cores but are powered completely by gravitational energy.

3.4. *Systematic Uncertainties*

The one system with a poor model fit, i.e. ID-5898, converges toward a solution with a high-mass secondary $M_2 = 3.8\,M_\odot$ ($q = 0.49$), young age $\tau \approx 0.8$ Myr, and small dust extinction $A_I = 0.07$. We find four reasons to suspect this system suffers from contamination with a third light source, most likely a hot late-B/early-A tertiary companion. First, the amplitude of the reflection effect in ID-5898 appears to be color dependent with $\Delta I_{\rm refl} = 0.10$ mag and $\Delta V_{\rm refl} = 0.07$ mag (see Fig. 5). The decrease in $\Delta V_{\rm refl}$ is most likely caused by stellar blending with a third light source that is relatively hot and brighter in the V-band. Second, the measured dust extinction $A_I = 0.07$ is smaller than that compared to dust reddening estimates of young stars along similar lines-of-sight (Zaritsky et al. 2004, see also below). Third light contamination from a hot source would artificially shift the observed color toward the blue and bias our dust reddening measurement toward smaller values. Third, extra light would diminish the primary eclipse depth ΔI_1. This would mainly lead to an underestimation of the inclination i, but may also cause us to overestimate L_2, R_2, and M_2. Considering the other 21 companions have $L_2 \lesssim 20\,L_\odot$, $R_2 \lesssim 5.2\,R_\odot$, and $M_2 \lesssim 2.4\,M_\odot$, the measurements of $L_2 \approx 180\,L_\odot$, $R_2 \approx 6.3\,R_\odot$, and $M_2 \approx 3.8\,M_\odot$ for ID-5898 are clear outliers and indicative of third light contamination. Finally, because third light contamination can bias our light curve solution to larger L_2 and R_2, our measured τ is also shifted toward younger ages. Of the four eclipsing binaries in our sample with age estimates $\tau \lesssim 1$ Myr, only ID-5898 is not embedded in a bright and/or compact H II region (see §4).

Considering the above, we remove ID-5898

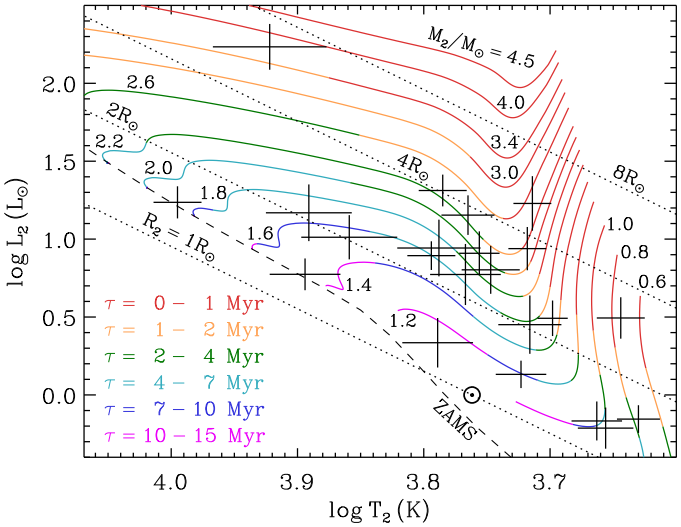

FIG. 6.— Hertzsprung-Russell diagram of the companions in our 22 eclipsing binaries. We compare the dependent model properties T_2 and L_2 to the Pisa pre-MS tracks (Tognelli et al. 2011) used to constrain the parameters of the observed systems. We display evolutionary tracks for secondary masses $M_2 = 0.6\text{-}4.5\,M_\odot$, where the colors indicate the ages of the pre-MS stars. We also show lines of constant radius (dotted) and the zero-age MS (dashed). ID-5898, which has the worst model fit statistic $\chi^2/\nu = 1.27$ and is probably contaminated by a third light source, is toward the top left. The three systems to the bottom left (ID-1965, ID-5377, and ID-6630) have small reflection effect amplitudes $\Delta I_{\rm refl} = 0.017\text{-}0.20$ mag, shallow eclipses $\Delta I_1 = 0.2$ mag, and companions that are consistent with the zero-age MS. The remaining 18 eclipsing binaries have companions that are larger and/or cooler and therefore definitively pre-MS stars. The observed systems cluster on the Henyey track near $T_2 \approx 6{,}000$ K and $L_2 \approx 10\,L_\odot$, which corresponds well to where large pre-MS stars with $R_2 \approx 2\text{-}4\,R_\odot$ are longest lived and therefore have the highest probability of producing detectable reflection effects.

when discussing correlations (§4) and the intrinsic binary fraction (§5). Nonetheless, ID-5898 is phenomenologically similar to the other 21 eclipsing binaries in our sample, and it most likely contains a low-mass pre-MS companion. We therefore still include this system in our total sample of 22 reflecting eclipsing binaries. We are simply unable to accurately constrain the physical properties of this system because of systematic effects most likely caused by third light contamination. Even if ID-5898 has a true mass ratio $q < 0.25$, the addition of this one object to the 19 measured systems with $q = 0.07$ - 0.25 would have a negligible effect on our statistics.

For each of our 22 eclipsing binaries, we calculate the covariance matrix and measurement uncertainties in our eight physical model parameters. However, most of our measured physical properties are dominated by systematic errors. In the following, we quantify the magnitudes and directions of various sources of systematic errors:

1. Bolometric corrections. For our hot B-type MS primaries, the bolometric corrections are large and typically uncertain by 0.2 - 0.3 mag (Pecaut & Mamajek 2013). This dictates the primary luminosities L_1 are uncertain by at least ≈20 - 30%, and therefore the inferred primary masses M_1 have systematic uncertainties of at least ≈10%. However, if we were to systematically overestimate or underestimate M_1, we would also bias our inferred M_2 in the same direction. This is because the measured ratio of eclipse depths $\Delta I_2/\Delta I_1$ mainly determines the luminosity contrast L_2/L_1 and therefore the mass ratio $q = M_2/M_1$. Hence, our measured mass ratios q are relatively insensitive to the uncertainties in the bolometric corrections.

2. Color indices. Given a surface temperature T_2, the intrinsic colors $(V-I)_o$ of hot B-type MS stars are uncertain by ≈0.02 mag (Pecaut & Mamajek 2013). The zero-point calibrations in the measured OGLE-III LMC colors are also uncertainty by ≈0.01 - 0.02 mag (Udalski et al. 2008). Our measured dust extinctions A_I therefore have a minimum systematic error of ≈0.03 mag.

3. Dust reddening law. The coefficient in our adopted dust reddening law $E(V-I) = 0.7A_I$ has a systematic error of ∼10% (Cardelli et al. 1989; Fitzpatrick 1999; Ngeow & Kanbur 2005). The inferred dust extinctions A_I are also uncertain by this factor.

4. Evolutionary tracks. Given a luminosity L_1 of the primary B-type MS star, the primary masses are uncertain by ≈10% according to the stellar evolutionary tracks (Dotter et al. 2008; Bertelli et al. 2009). Rotating models of young B-type MS stars are only 4% cooler than their non-rotating counterparts (Ekström et al. 2008a). This implies a 5% systematic uncertainty in the masses of the B-type MS stars due to the uncertainty in the rotation rates. For the pre-MS companions in our eclipsing binaries, we compare pre-MS models based on four different calculations (Siess et al. 2000; Dotter et al. 2008; di Criscienzo et al. 2009; Tognelli et al. 2011). For ages $\tau \gtrsim 1$ Myr and masses $M_2 > 1.3$, all pre-MS evolutionary tracks agree fairly well with typical errors of ≈15% in mass and ≈25% in age. At younger ages and lower masses, the systematic uncertainties increase to $\delta\tau \approx 0.3$ Myr and $\delta M_2 \approx 0.2 M_\odot$.

5. Irradiation effects. The luminosity received by the pre-MS companion from the B-type MS star is comparable to the intrinsic luminosity of the pre-MS star itself. This may cause the companion to enlarge, especially if it has a convective envelope and the albedo is measurably less than unity. This effect has been studied in the context of low-mass X-ray binaries in which a hot accretion disk around a compact object irradiates a cool, low-mass donor (Podsiadlowski 1991; Ritter et al. 2000). If the irradiation effects are on one side, as they are in X-ray binaries as well as in our eclipsing binaries, then the radius of the companion increases by only ≈5% (Ritter et al. 2000). Instead of becoming stored in the interior of the star, the intercepted energy quickly diffuses laterally to the unirradiated side and subsequently lost via radiation. This ≈5% systematic effect in radius is smaller than the uncertainties due to the evolutionary tracks discussed above. Most importantly, irradiation effects would shift the pre-MS companions toward larger radii and luminosities, so that we would have overestimated, not underestimated, their masses. Our conclusion that the companions in our eclipsing binaries are low-mass pre-MS stars is therefore not affected by irradiation effects.

6. Zero-point age calibration. Although our eclipsing binaries are detached from their Roche lobes and are currently evolving relatively independently from each other, they most likely experienced prior coevolution. In particular, the two components probably competed for accretion in the same circumbinary disk (Bate et al. 2002). Isolated T Tauri pre-MS stars with masses ≈ 1 - $3\,M_\odot$ still have thick circumstellar disks at ages $\tau \approx 0.5$ - 5 Myr (Hartmann 2009). There is no evidence for circumstellar disks in the photometric light curves of our 22 eclipsing binaries in the LMC as we observe in nearby BM Orionis (Windemuth et al. 2013, see §2). The absence of circumstellar disks in our eclipsing binaries demonstrates that the pre-MS companions formed differently than they would have in isolation. Nonetheless, most of the mass of a solar-type star is accreted at very early stages $\tau \lesssim 0.2$ Myr (Hartmann 2009). Moreover, the theoretical evolutionary tracks (Siess et al. 2000; Dotter et al. 2008; di Criscienzo et al. 2009; Tognelli et al. 2011) assume pre-MS stars evolve with constant mass, which better describe our low-mass pre-MS companions without disks than isolated low-mass pre-MS stars with disks.

   The time of initial pre-MS contraction and observability, sometimes called the birthline (Palla & Stahler 1990), can differ by 0.2 Myr between components in the same binary system (Stassun et al. 2008). Fortunately, the initial contraction phases are extremely rapid, and so the zero-point age calibration is uncertain by at most ≈0.4 Myr (see also fourth

item in this list). Finally, we measured the ages τ and masses M_2 of the *companions* according to their properties T_2 and R_2 (Fig. 6). We inferred these companion properties from T_1, R_1, and the light curve characteristics. Because T_1 and R_1 of the B-type MS primaries evolve much more slowly than T_2 and R_2 of the low-mass pre-MS companions, then our models are not too sensitive to the age of the primary. Even if the primary was slightly older or younger than the companion, we would still measure the same age τ and mass M_2 for the secondary. In short, the current properties of our pre-MS companions with ages $\tau > 0.6$ Myr are primarily dictated by their masses, with little dependence on the presence of a disk, prior coevolution at $\tau \lesssim 0.4$ Myr, or age of the primary.

7. Eclipsing binary models. For the same physical parameters, we compare our best-fit models produced by NIGHTFALL with light curves generated by the eclipsing binary software PHOEBE (Prša & Zwitter 2005). We find only slight differences, typically caused by the different treatment of limb-darkening and albedo between the two packages.

8. Third light contamination. Our measured physical properties can deviate beyond the calculated uncertainties if the photometric light curves include a third light source that is brighter than $\gtrsim$10% the luminosity of the B-type MS primary. In Moe & Di Stefano (2013), we measured the spatial density of bright stars, typically giants, in the LMC. We determined the probability that a luminous B-type MS eclipsing binary is blended with such a bright foreground or background star is only $\approx$5%. Most close binaries are orbited by an outer tertiary component (Tokovinin et al. 2006), but wide companions are weighted toward small mass ratios (Abt et al. 1990; Shatsky & Tokovinin 2002). Hence, the probability that our eclipsing binaries are orbited by a bright, massive late-B/early-A tertiary component is only ≈10% (Moe & Di Stefano 2013). Given our sample of 22 reflecting eclipsing binaries, we expect only one to be blended with a background or foreground cool giant, and possibly two to contain a hot luminous tertiary companion. ID-5898 probably experiences the latter of these two types of third light contamination. In addition, our model for ID-7419 results in a moderately poor fit statistic $\chi^2/\nu = 1.20$, low inclination $i \approx 81^{\rm o}$, and large dust extinction $A_I \approx 0.7$ mag. ID-7419 is most likely contaminated with a cool foreground or background giant. Third light contamination causes us to overestimate, not underestimate, the secondary masses M_2, and typically results in larger χ^2/ν statistics. Most importantly, third light contamination affects only two to three individual systems in our sample, not our entire population like the previously discussed sources of systemic errors.

Based on the above, we add in quadrature to our statistical measurement uncertainties the following systematic errors. M_1: 15% relative error; M_2: 15% relative error or absolute error of $0.2\,{\rm M}_\odot$, whichever is larger; τ: 25% or 0.4 Myr, whichever is larger; and A_I: 10% or 0.03 mag, whichever is larger. We propagate these systematic uncertainties in M_1, M_2, τ, and A_I into the other model parameters P, $t_{\rm o}$, i, and A_2 according to the covariance matrix. In Table 2, the values in parenthesis represent the total uncertainties, including systematic errors, in the final decimal places of our eight model parameters. Note that we list the best-fit model parameters in Table 2, and so the reported uncertainties are not necessarily symmetric around the best-fit values. The uncertainties in P and $t_{\rm o}$ primarily derive from the observed light curves with little contribution from the systematic errors. The uncertainties in the secondary albedos A_2 are quite large, but the other physical properties are relatively independent of this parameter. Typical errors in the mass ratios q and relative ages $\tau/\tau_{\rm MS}$ are 15% or 0.03, whichever is larger. The uncertainties in the luminosities L_1 and L_2 are ≈40%, which are primarily due to the systematic uncertainties in the bolometric corrections discussed above. Given the precisely measured orbital periods and the uncertainties in the masses and evolutionary tracks, the uncertainties in the orbital separations a, radii R_1 and R_2, and Roche-lobe fill-factors $RLFF_1$ and $RLFF_2$ are ≈10% according to Kepler's third law. Finally, given the uncertainties in the radii and luminosities, the representative errors in the temperatures T_1 and T_2 are ≈8% according to the Stefan-Boltzmann law. Although the systematic errors dominate our total uncertainties, our conclusions that 19 of our eclipsing binaries with reflection effects have small mass ratios $q \lesssim 0.25$ and young ages $\tau \lesssim 15$ Myr are robust.

As a consistency check, we compare our fitted dust reddening measurements $E(V-I) = 0.7A_I$ to the Zaritsky et al. (2004) LMC dust reddening maps. Specifically, we compile the Zaritsky et al. (2004) A_V values toward hot, young LMC stars within one arcminute of each of our 22 eclipsing binaries. We typically find ≈10 - 25 such systems in their database that are this close to our eclipsing binaries. For each area, we calculate the mean extinction and standard deviation of the mean extinction. We convert these V-band extinction values into dust reddenings $E(V-I) = 0.41A_V$ using are adopted reddening law. Finally, we add in quadrature to the measurement uncertainties a systematic error of 0.03 mag (see second item in list above). In Fig. 7, we compare our values and uncertainties for $E(V-I)$ to those we compiled from Zaritsky et al. (2004). Only ID-5989 and ID-7419, which have the largest χ^2/ν statistics most likely caused by third light contamination, have dust reddening measurement that are discrepant with the Zaritsky et al. (2004) values. As discussed above, third light contamination will bias our dust reddening measurements toward larger or smaller values, depending on the color of the third light source. For the remaining 20 of our eclipsing binaries, the two dust reddening estimates are in agreement, which demonstrates the reliability of our eclipsing binary models.

4. ASSOCIATION WITH H II REGIONS

Because our eclipsing binaries with reflection effects contain pre-MS companions, they should be systematically younger than their non-reflecting

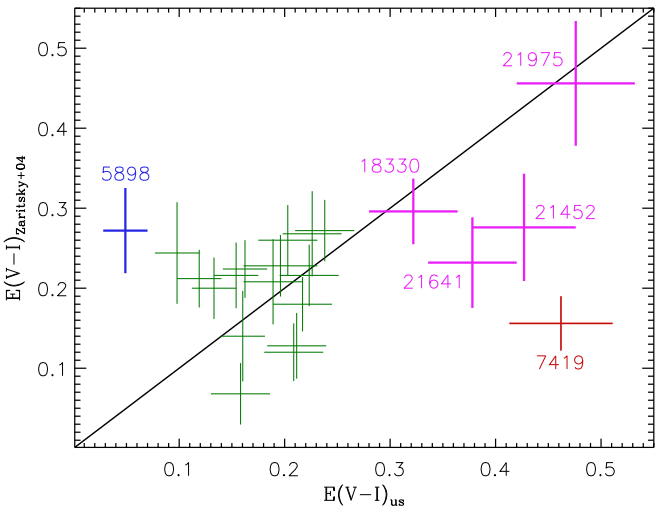

FIG. 7.— Comparison of our fitted dust reddening measurements to values obtained by Zaritsky et al. (2004) of hot young stars along similar lines-of-sight to our 22 nascent eclipsing binaries. The majority of systems (green) are only slightly reddened with $E(V-I) \approx 0.1$ - 0.3. The four highly reddened eclipsing binaries (magenta) with $E(V-I) \approx 0.3$ - 0.5 are in the eastern portions of the LMC and embedded in bright, dusty H II regions, e.g. ID-21452 is in 30 Doradus. The two systems that deviate more than 3σ from the Zaritsky et al. (2004) measurements, ID-5989 (blue) and ID-7419 (red), happen to be the two eclipsing binaries with the poorest model fits to the observed light curves, $\chi^2/\nu = 1.27$ and $\chi^2/\nu = 1.20$, respectively. This indicates third light contamination dominates the systematic errors in these two systems, while the other 20 eclipsing binaries are relatively free from third light contamination.

counterparts. To test this prediction, we check for correlations between the coordinates of the eclipsing binaries and positions of star-forming H II regions in the LMC. In Table 4, we list various properties of our 22 eclipsing binaries, including their identification numbers and coordinates from the OGLE-III LMC eclipsing binary catalog (Graczyk et al. 2011). To perform our statistical analysis below, we utilize the coordinates, sizes, and position angles of the 1,164 H II regions in the Bica et al. (1999) catalog designated as class NA or NC, i.e. stellar associations and clusters, respectively, clearly related to emission nebulae. We report in Table 4 the properties of the H II regions with which 20 of our reflecting eclipsing binaries are associated. This includes the projected offset r (in pc) between the eclipsing binaries and the centers of the H II regions, the physical radii $\langle r \rangle_{\rm H\,II}$ (in pc) of the H II regions, and the H II region catalog identification numbers and names from Bica et al. (1999). We define the mean physical radius to be $\langle r \rangle_{\rm H\,II} = \sqrt{A \times B}/2$, where A and B are the major and minor axes provided by Bica et al. (1999) projected at the distance $d = 50$ kpc to the LMC.

In Fig. 8, we show the coordinates of the 2,206 B-type MS eclipsing binaries in our full sample, and the 22 systems that exhibit reflection effects with large, pre-MS companions. In the background of Fig. 8, we display an image of the LMC taken from the Magellanic Cloud Emission Line Survey (Smith et al. 2005), where the star-forming H II regions are clearly visible. Based on the Bica et al. (1999) catalog, only 16% of normal B-type MS eclipsing binaries have projected distances $r < 30$ pc from the centers of H II regions. In contrast, 13 of our 22 systems with reflection effects, i.e. $(59 \pm 10)\%$, are situated this close to such stellar nurseries. These values differ at the 4.1σ significance level, demonstrating that B-type MS eclipsing binaries with reflection effects are dramatically younger.

Similarly, only 4.8% of B-type MS eclipsing binaries are located in centrally condensed H II regions with mean physical radii $\langle r \rangle_{\rm H\,II} = 3$ - 30 pc. Meanwhile, 10 of the 22 systems with reflection effects, i.e. $(45 \pm 11)\%$, are embedded in such star-forming environments. In addition, 10 of the remaining 12 reflecting eclipsing binaries are associated with extended, more diffuse H II regions with $\langle r \rangle_{\rm H\,II} > 30$ pc. These statistics demonstrate that our B-type MS eclipsing binaries with reflection effects are relatively young with ages $\tau \approx 1$ - 8 Myr that are comparable to the lifetimes of H II regions.

Only 2 of our 22 eclipsing binaries with reflection effects do not appear to be associated with an H II region. One of these systems, ID-5377, is relatively old at $\tau = 14 \pm 5$ Myr (Table 4), and so it is not unexpected that it is relatively remote from a site of active star formation. In contrast, the other eclipsing binary that is not in an H II region, ID-9642, is relatively young at $\tau = 1.7 \pm 0.5$ Myr. We speculate that this eclipsing binary with a B-type MS primary may have formed in relative isolation without nearby O-type stars to ionize the surrounding gas (see de Wit et al. 2004; Parker & Goodwin 2007). As another possibility, the young ID-9642 may be embedded in a compact H II

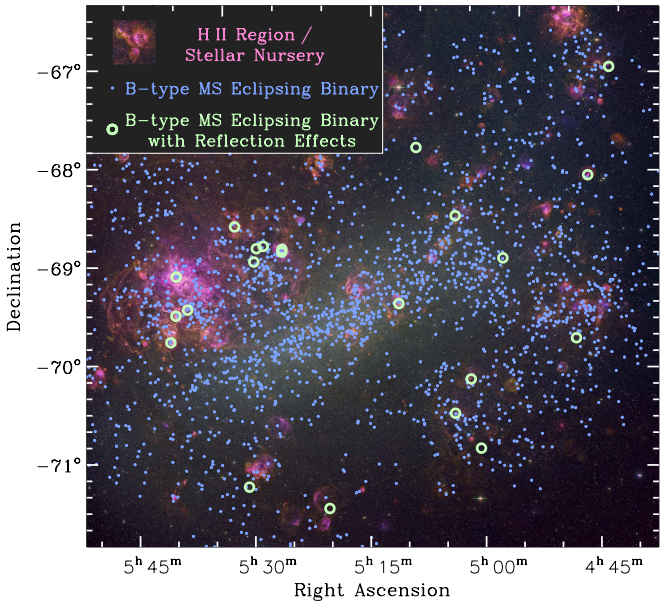

FIG. 8.— The positions of the 2,206 eclipsing binaries with B-type MS primaries and orbital periods $P = 3$ - 15 days (blue dots) and the subset of 22 systems that exhibit pronounced reflection effects with pre-MS companions (green circles) superimposed on a narrow-band color image of the LMC taken from the Magellanic Cloud Emission Line Survey (Smith et al. 2005). The largest concentration of normal B-type MS eclipsing binaries is in the central bar of the LMC, while those displaying reflection effects typically reside in star-forming H II regions. Relative to their non-reflecting counterparts, the positions of our 22 reflecting eclipsing binaries are correlated with the positions of H II regions at the 4.1σ confidence level. This demonstrates our 22 eclipsing binaries that exhibit reflection effects are systematically younger, which reinforces our conclusion that they contain low-mass pre-MS secondaries.

Table 4. Coordinates and properties of the 22 eclipsing binaries with reflection effects, and their association with H II regions.

ID	RA (J2000)	DE (J2000)	ΔI_1	$\Delta I_{\rm refl}$	τ (Myr)	r (pc)	$\langle r \rangle_{\rm H\,II}$ (pc)	H II ID	H II Name
1803	4h 51m 58.23s	−66° 57′ 00.0″	0.64	0.138	0.7	25	8	351	NGC1714 in Shapley-VI
1965	4h 52m 34.89s	−69° 42′ 24.7″	0.20	0.017	15	140	400	470	SGshell-LMC7
2139	4h 53m 05.17s	−68° 03′ 03.4″	0.33	0.033	0.9	3	6	418	HDE268680 in NGC1736
5377	5h 01m 44.99s	−68° 53′ 43.2″	0.17	0.020	14				
5898	5h 02m 58.72s	−70° 49′ 44.7″	0.83	0.098	0.8	380	400	1172	Shapley-VIII
6630	5h 04m 39.43s	−70° 07′ 33.3″	0.16	0.019	13	19	26	1331	BSDL552 in LMC-DEM68
7419	5h 06m 21.44s	−70° 28′ 27.5″	0.19	0.037	5.2	290	400	1172	Shapley-VIII
7842	5h 07m 17.97s	−68° 28′ 03.8″	1.73	0.083	2.6	5	16	1572	BSDL657 in LMC-DEM76
9642	5h 11m 46.29s	−67° 46′ 25.1″	0.70	0.050	1.7				
10289	5h 13m 23.92s	−69° 21′ 37.3″	0.20	0.034	2.5	6	11	2124	NGC1876 in SL320
13721	5h 21m 51.38s	−71° 26′ 31.5″	0.42	0.025	8	80	120	3018	LMC-DEM164 in SGshell-LMC9
15761	5h 26m 35.54s	−68° 48′ 35.7″	0.85	0.108	1.9	5	3	3598	LMC-N144B in SL476
15792	5h 26m 37.37s	−68° 50′ 09.2″	0.23	0.039	2.8	17	11	3635	NGC1970 in SL476
16828	5h 28m 40.41s	−68° 46′ 42.8″	0.11	0.018	7	170	200	3759	Shapley-II in SGshell-LMC3
17217	5h 29m 27.69s	−68° 48′ 09.9″	0.10	0.022	7	180	200	3759	Shapley-II in SGshell-LMC3
17387	5h 29m 49.28s	−68° 56′ 17.6″	0.09	0.017	8	150	200	3759	Shapley-II in SGshell-LMC3
18330	5h 31m 44.95s	−68° 34′ 52.5″	0.30	0.056	5.6	11	11	4256	BSDL2159 in LMC-DEM227
18419	5h 31m 55.78s	−71° 13′ 32.0″	0.55	0.059	1.6	30	4	4389	LMC-N206D in SGshell-LMC9
21025	5h 37m 45.75s	−69° 25′ 38.8″	0.13	0.025	6	48	56	5056	LMC-DEM261 in LH96
21452	5h 38m 43.99s	−69° 05′ 29.6″	2.82	0.124	0.6	8	26	5112	30 Doradus in NGC2070
21641	5h 39m 10.90s	−69° 29′ 20.2″	0.41	0.062	2.6	12	27	5140	NGC2074 in LMC-N158
21975	5h 40m 03.86s	−69° 45′ 32.3″	0.14	0.030	4.0	5	10	5252	NGC2084e in LMC-N159

region with $\langle r \rangle_{\rm H\,II} \lesssim 1$ pc that is below the resolution limit of ground-based surveys and therefore not in the Bica et al. (1999) catalog. In any case, the fact that 20 our our 22 eclipsing binaries are associated with H II regions reinforces our conclusion that the majority of the companions are young, low-mass, pre-MS stars.

The positions of our 22 eclipsing binaries and their associations with H II regions also corroborate the reliability of our eclipsing binary models. For example, ID-15761 and ID-15792 are both associated with the same H II region SL476. For these two systems, we derived ages $\tau = 1.9 \pm 0.5$ Myr and $\tau = 2.8 \pm 1.0$ Myr, respectively, that are consistent with each other, and dust extinctions $A_I = 0.30 \pm 0.04$ mag that match each other. Similarly, ID-16828, ID-17217, and ID-17387 are all in the large diffuse H II region Shapley-II with $\langle r \rangle_{\rm H\,II} \approx 200$ pc. These three eclipsing binaries have slightly older ages $\tau \approx 7$ - 8 Myr and consistently smaller dust extinctions $A_I \approx 0.23$ - 0.28 mag. Our youngest three eclipsing binaries with reliable age estimates $\tau \lesssim 1$ Myr, i.e. ID-1803, ID-2139, and ID-21452, are all associated with centrally condensed H II regions with $\langle r \rangle_{\rm H\,II} \lesssim 30$ pc. Alternatively, our three oldest systems with $\tau \approx 13$ - 15 Myr and companions close to the zero-age MS, i.e. ID-1965, ID-5377, and ID-6630, are either not associated with star-forming environments or are in relatively large and/or diffuse H II regions.

We now examine these correlations between eclipsing binary parameters and the properties of the H II regions in which they reside in a more statistical manner. In Table 4, we list the observed primary eclipse depths ΔI_1 and reflection effect amplitudes $\Delta I_{\rm refl}$ from Table 1, and the modeled ages τ from Table 2. The uncertainties in the primary eclipse depths are dominated by systematic errors $\delta \Delta I_1 \approx 0.01$ mag, except for the two systems with the deepest eclipses that have $\Delta I_1 = 1.73 \pm 0.05$ mag (ID-7842) and $\Delta I_1 = 2.82 \pm 0.14$ mag (ID-21452). The uncertainties in the reflection effect amplitudes are $\delta \Delta I_{\rm refl} \approx 0.003$ mag, and the uncertainties in the ages τ are as those reported in Table 2.

In Fig. 9, we compare the eclipsing binary properties listed in Table 4, where we have excluded ID-5898 which is most likely biased toward shallower eclipses and younger ages due to third light contamination. The empirical properties of primary eclipse depth ΔI_1 and reflection effect amplitude $\Delta I_{\rm refl}$ are positively correlated (Spearman rank correlation coefficient $\rho = 0.85$) at a statistically significant level (probability of no correlation $p = 2{\times}10^{-6}$). This is because both ΔI_1 and $\Delta I_{\rm refl}$ are inextricably linked to the radius R_2 of the pre-MS companion. The age τ is anti-correlated with both ΔI_1 and $\Delta I_{\rm refl}$ ($\rho = -0.70$ and $\rho = -0.83$, respectively) because older pre-MS stars are systematically smaller. Although still statistically significant ($p = 3{\times}10^{-6}$ - $4{\times}10^{-4}$), these correlations are not as strong because the radius of a pre-MS star also depends on its mass in addition to its age.

The three properties ΔI_1, $\Delta I_{\rm refl}$, and τ of the eclipsing binaries are all significantly correlated with the mean physical radii $\langle r \rangle_{\rm H\,II}$ of the H II regions with which they are associated. Namely, younger eclipsing binaries with deeper primary eclipses and larger reflection effect amplitudes are typically embedded in bright and/or condensed H II regions. These correlations are statistically significant ($p = 5{\times}10^{-4}$ - 0.01), but the mapping between the eclipsing binary properties and the radii of the H II regions are not one-to-one ($|\rho| \approx 0.6$ - 0.7). For example, ID-21452, which happens to be our youngest system ($\tau = 0.6 \pm 0.4$ Myr) with the deepest eclipse ($\Delta I_1 \approx 2.8$ mag), resides in the famous, bright, large H II region 30 Doradus (also known as the Tarantula Nebula; RA $\approx 5^{\rm h}39^{\rm m}$ and DE $\approx -69.1°$ in Fig. 8). Such large, bright H II regions can host multiple episodes of star formation (Crowther 2013). Specifically, 30 Doradus contains an older population of stars with $\tau = 20$ - 25 Myr, which is consistent with its larger size, and a more recent generation that is $\tau \lesssim 1$ - 2 Myr old, which is consistent with the age derived for ID-21452 (Massey & Hunter 1998; Grebel & Chu 2000).

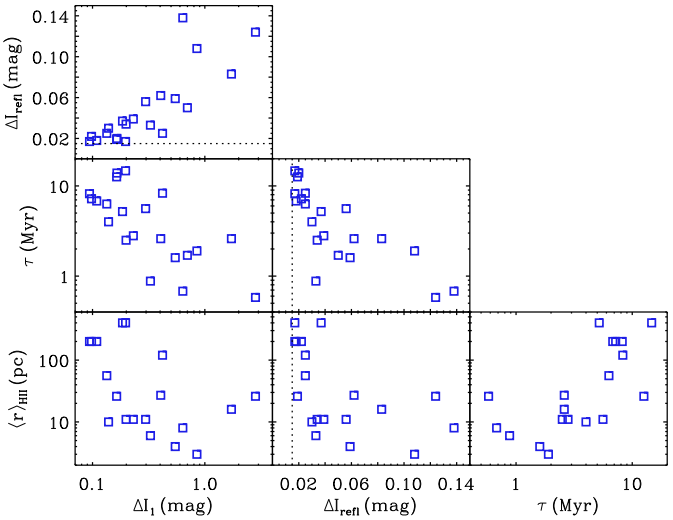

FIG. 9.— Properties of eclipsing binaries and H II regions. The reflection effect amplitudes $\Delta I_{\rm refl}$, primary eclipse depths ΔI_1, ages τ, and physical radii of the H II regions $\langle r \rangle_{\rm H\,II}$ in which the eclipsing binaries reside are all correlated with each other at a statistically significant level. Our eclipsing binaries provide powerful diagnostics and constraints for the dynamical evolution and expansion velocities $\langle v \rangle_{\rm H\,II} \approx 10$ - 30 km s^{-1} of H II regions. See text for details and a discussion of uncertainties.

The properties of our nascent eclipsing binaries provide powerful diagnostics for the long-term evolution of H II regions. Namely, the mean expansion velocity $\langle v \rangle_{\rm H\,II} = \langle \langle r \rangle_{\rm H\,II} / \tau \rangle$ of H II regions derives from the slope of the observed correlation in the bottom right panel of Fig. 9. For the 12 bright and centrally condensed H II regions with $\langle r \rangle_{\rm H\,II} = 3$ - 30 pc, we find a mean expansion velocity of $\langle v \rangle_{\rm H\,II} = 8 \pm 3$ km s^{-1}. This is consistent with both observed and theoretical estimates of $\langle v \rangle_{\rm H\,II} \approx 10$ km s^{-1} during the subsonic expansion phase of H II regions when $\tau \approx 0.01$ - 5 Myr (Yorke 1986; Cichowolski et al. 2009). For the seven large and diffuse H II regions with $\langle r \rangle_{\rm H\,II} > 30$ pc, we calculate $\langle v \rangle_{\rm H\,II} = 29 \pm 8$ km s^{-1}. This coincides with the observed range of expansion velocities $v \approx 15$ - 45 km s^{-1} in giant H II shell-like regions within nearby galaxies (Chu & Kennicutt 1994; Tomita et al. 1998). Our ability to measure the ages of several eclipsing binaries to accuracies of ≈25% give tight constraints for the dynamical evolution of the H II regions in which they formed.

5. THE INTRINSIC CLOSE BINARY STATISTICS

In the following, we determine the intrinsic fraction F of B-type MS stars that have close low-mass companions. We utilize the properties and statistics of our nascent eclipsing binaries, and so we must correct for geometrical and evolutionary selection effects in our magnitude-limited sample. To achieve this, we estimate the probability density functions (§5.1) for the eight parameters in §3 that describe our physical models. With these distributions, we calculate the probability of observing reflection effects using two approaches: a simple estimate (§5.2) and a detailed Monte Carlo simulation (§5.3 - 5.4).

5.1. *Probability Density Functions*

The distribution of dust extinction toward B-type MS stars in the LMC peaks at $A_V \approx 0.4$ mag, i.e. $A_I \approx 0.2$ mag according to our adopted reddening law, with a long tail toward larger values (Zaritsky 1999; Zaritsky et al. 2004). To match these observations, we utilize a beta probability distribution to model the extinction distribution in the I-band:

$$p_{A_I} = 30 A_I (1 - A_I)^4 \quad \text{for } 0 < A_I < 1, \qquad (7)$$

where A_I is in magnitudes. The measured dust extinctions A_I of our 22 reflecting eclipsing binaries are also consistent with this distribution (see Table 2 and Fig. 7).

To quantify the probability density functions for M_1 and τ, we estimate the initial mass function (IMF) and recent star-formation history (SFH) within the OGLE-III footprint of the LMC. We consider a single power-law IMF for massive primaries:

$$dN = k M_1^{-\alpha} dM_1 \quad \text{for } 3\,M_\odot < M_1 < 30\,M_\odot \qquad (8)$$

where the normalization constant k and IMF slope α are free parameters. Note that $\alpha = 2.35$ corresponds to the standard Salpeter value. We model the relative SFH of the LMC for ages $0\,{\rm Myr} < \tau < 320\,{\rm Myr}$, where $\tau = 320$ Myr is the MS lifetime of the lowest mass primaries $M_1 = 3\,{\rm M}_\odot$ we have considered. We set the relative star-formation rate during recent times $0\,{\rm Myr} < \tau < 10\,{\rm Myr}$ to unity, and consider five free parameters A-E to describe the SFH at earlier epochs:

$$SFH(\tau) = \begin{cases} 1 & \text{for } 0\,{\rm Myr} \le \tau < 10\,{\rm Myr} \\ A & \text{for } 10\,{\rm Myr} \le \tau < 20\,{\rm Myr} \\ B & \text{for } 20\,{\rm Myr} \le \tau < 40\,{\rm Myr} \\ C & \text{for } 40\,{\rm Myr} \le \tau < 80\,{\rm Myr} \\ D & \text{for } 80\,{\rm Myr} \le \tau < 160\,{\rm Myr} \\ E & \text{for } 160\,{\rm Myr} \le \tau < 320\,{\rm Myr} \end{cases} \qquad (9)$$

To measure the IMF and SFH model parameters, we utilize the observed present-day luminosity function of MS stars in the OGLE-III LMC database (Udalski et al. 2008). In Fig. 10, we show the observed magnitude distribution across $15.0 < \langle I \rangle < 18.0$ for early-type MS systems with $-0.25 < \langle V - I \rangle < 0.20$. We have extended our magnitude range to include brighter, short-lived O-type primaries to better constrain the more recent SFH within the OGLE-III LMC footprint.

To account for systematic errors caused by unresolved binary stars in the OGLE-III LMC database, we consider two models. For Model 1, we assume all stars are single, and so the magnitude $\langle I \rangle$ and color $\langle V - I \rangle$ of a system is simply determined by M_1, τ, and A_I according to our adopted stellar tracks. For Model 2, we assess the bias in the luminosity distribution due to companions $q \gtrsim 0.7$ that are comparable in mass and luminosity to the primary. This bias in the luminosity distribution of binary stars was first discussed by Öpik (1923), and we have previously investigated this Öpik effect in the context of stellar populations in extragalactic environments (Moe & Di Stefano 2013). In short, we must approximate the total fraction of B-type MS stars with companions $q \gtrsim 0.7$ across all orbital periods that can measurably affect the luminosity

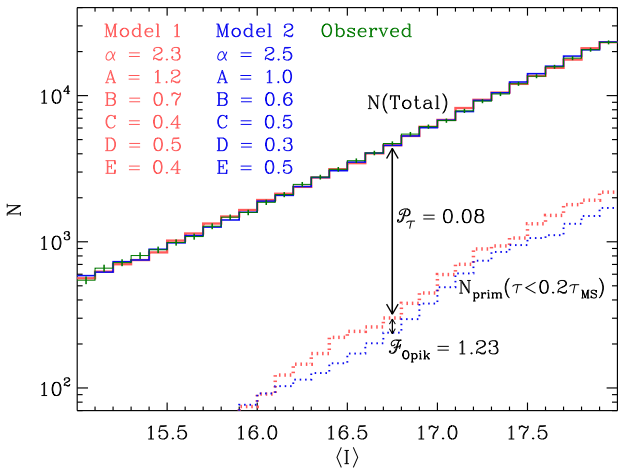

FIG. 10.— Present-day luminosity function of MS stars in the LMC. We compare the $\langle I \rangle$ distribution of MS systems with $-0.25 < \langle V-I \rangle < 0.20$ in the OGLE-III LMC database (green) to simulated models assuming all systems are single stars (Model 1 - red) or binaries (Model 2 - blue). We find similar fit parameters between these two models for the slope α of the IMF and relative rates A - E of star formation. For our simulated stellar populations, we also display the predicted number of primaries with ages that are <20% their MS lifetimes (dotted). In a magnitude-limited sample, only $\mathcal{P}_\tau \approx 8\%$ of systems are young enough to have pre-MS companions that are capable of producing detectable reflection effects. In a population of binaries that contain companions $q \gtrsim 0.7$ that are comparable in mass and luminosity to the primary, the total luminosity function is biased toward these bright binaries according to the Öpik effect. Hence, there are *fewer* total primaries by a factor of $\mathcal{F}_{\rm Opik} = 1.23 \pm 0.10$.

of the system. For Model 2, we therefore assume a 100% total binary star fraction and an overall mass-ratio distribution $p_q \propto q^{-0.4}\,dq$ across $0.05 < q < 1.0$, which is consistent with current observations of B-type MS stars (Kobulnicky & Fryer 2007; Kouwenhoven et al. 2007; Rizzuto et al. 2013). The companion star fraction may exceed 100% for B-type MS stars, but this is most likely at the expense of increasing the number of low-mass tertiaries that are not easily detectable. Hence, the fraction of B-type MS primaries that have luminous companions $q \gtrsim 0.7$ is robust at (23 ± 10)%.

By implementing a Monte Carlo technique, we generate a population of stars (Model 1) or binaries (Model 2) using our adopted evolutionary stellar tracks and models for the IMF, SFH, and dust extinction distribution. To constrain the IMF and SFH model parameters, we minimize the χ^2 statistic between the observed and simulated present-day $\langle I \rangle$ distributions (see Fig. 10). For both models, we measure a primary star IMF that is consistent with the Salpeter value. We also find that the star-formation rate has been relatively constant over the past $\approx$20 Myr, but was $\approx$40% the present-day value at earlier epochs $\tau > 80$ Myr. This is consistent with other measurements of the SFH in the LMC (Harris & Zaritsky 2009; Indu & Subramaniam 2011). The uncertainties in the overall binary properties have little influence on our derived slope of the IMF or the relative SFH. We therefore adopt parameters between our two models, namely $\alpha = 2.4$, $A = 1.1$, $B = 0.7$, $C = 0.5$, and D=E=0.4.

Only the normalization constant between our single and binary star populations significantly differ. For our binary population, we measure $\approx$20% fewer systems due to the Öpik effect. We also find 20% more total mass in our binary population because the average binary contains $\approx$1.4 times the mass of the primary, i.e. $\langle q \rangle \approx 0.4$. When we generate synthetic eclipsing binary light curves (§5.3), we simulate only systems that are similar to our 22 observed eclipsing binaries. Quantitatively, we generate only B-type MS stars with low-mass companions $q = 0.06$ - 0.40 at short orbital periods $P = 3.0$ - 8.5 days. We therefore need to correct for the luminosity bias of $q \gtrsim 0.7$ companions. Because the observed luminosity distribution is biased toward these binaries with equally bright components, the distribution is biased *against* single stars as well as binaries with faint, low-mass companions $q \lesssim 0.7$. We therefore multiply our calculated intrinsic fraction F of low-mass companions by a correction factor of $\mathcal{F}_{\rm Opik} = 1.23 \pm 0.10$ to account for this Öpik effect.

The probability density functions for the remaining physical model parameters are easier to quantify. We assume random epochs of primary eclipse minima t_o. We also assume random orbital orientations so that $\cos(i) = [0, 1]$ is uniformly distributed on this interval. We select secondary albedos from a uniform distribution across the interval $A_2 = [0.3, 1.0]$, which encompasses the range of observed albedos in our eclipsing binaries with reflection effects (see Table 3). Although the average albedo of this distribution $\langle A_2 \rangle = 0.65$ is slightly lower than the observed average $\langle A_2 \rangle \approx 0.71$, the latter is a posterior average and companions with higher albedos are more likely to be detected. Also, the albedo A_2 may be dependent on the effective temperature T_2 (Claret 2001), but small correlations between model parameters are second-order effects in our overall calculations. We assume log P is uniformly distributed across the interval $P = 3.0$ - 8.5 days, which is consistent with observations of binaries with B-type MS primaries (Abt et al. 1990; Kobulnicky & Fryer 2007; Kouwenhoven et al. 2007). Reasonable deviations from this distribution have little effect on our statistics, especially considering we are examining such a narrow window of orbital periods. Finally, in order to calculate the detectability of reflection effects as a function of mass ratio, we consider four logarithmic $d\log q = 0.2$ intervals across the total range log $q = -1.2$ - -0.4, i.e. $q = 0.06$ - 0.40. In our detailed Monte Carlo simulations, we treat each of these four mass-ratio bins independently, and select log q from a uniform distribution within each interval. Again, the precise distribution of mass ratios within each narrowly divided bin is inconsequential to our overall uncertainties.

5.2. *Simple Estimate*

Before we utilize a Monte Carlo technique to generate synthetic light curves for a population of eclipsing binaries, we first perform a simple calculation. Using the measured properties of our 22 eclipsing binaries, we estimate the probability $\mathcal{P}_{\rm refl}$ that a B-type MS primary and low-mass companion have the necessary configuration to produce observable eclipses and reflection effects. In this simple estimate, we do not account for all eight physical model parameters outlined above. Instead, we consider only the following three main selection effects.

First, eclipsing binaries must have nearly edge-on orientations so that the eclipses are deep enough to be observed given the sensitivity of the OGLE-III LMC observations. The observed eclipsing binaries with reflection effects in our sample generally have $i \gtrsim 80^{\rm o}$ (Table 2). This implies the probability of having sufficiently edge-on inclinations is $\mathcal{P}_i \approx \cos(80^{\rm o}) \approx 0.17$.

Second, the observed eclipsing binaries generally have short orbital periods. This is not only due to geometrical selection effects, but also because irradiation effects quickly diminish with orbital separation. The majority of our systems have P = 3.0 - 5.5 days, implying $\mathcal{P}_P \approx (\log 5.5 - \log 3.0)/(\log 8.5 - \log 3.0) \approx 0.6$ if the intrinsic distribution of orbital periods is uniform in $\log P$.

Finally, our reflecting eclipsing binaries must be young enough so that the companion is still on the pre-MS, but bright enough to be contained in our magnitude-limited sample. A B-type MS primary can have a pre-MS companion only if the age of the binary τ is a certain fraction of the primary's MS lifetime $\tau_{\rm MS}$. For moderate mass ratios $q \approx 0.25$, the ages must be $\tau \lesssim 0.1\ \tau_{\rm MS}$. For binaries with extreme mass ratios $q \approx 0.15$, close orbits P = 3 - 4 days, and bright massive primaries M_1 = 12 - 16 $\rm M_\odot$, we can discern reflection effects up to $\tau \approx 0.5\,\tau_{\rm MS}$ (Table 3, Fig. 4, and left panel of Fig. 11). For our simple estimation purposes, we adopt an average criterion that the binary must have an age $\tau < 0.2\,\tau_{\rm MS}$ in order for the companion to be a pre-MS star. One may initially assume that the probability of observing such a young binary is $\mathcal{P}_\tau = 0.2$, but this is not the case for our magnitude-limited sample. By incorporating our simulated stellar populations used to quantify the SFH and IMF above, we display in Fig. 10 the number of systems with primaries that have ages $\tau < 0.2\ \tau_{\rm MS}$ for each magnitude bin. The true probability that a system has such a young age is $\mathcal{P}_\tau = \mathcal{N}(\tau < 0.2\tau_{\rm MS})/\mathcal{N}({\rm total}) \approx 0.08$, which is a factor of 2 - 3 times lower than the crude estimate of $\mathcal{P}_\tau = 0.2$. Late-B MS primaries with $M_1 \approx$ 3 - 6 $\rm M_\odot$ can have observed magnitudes $\langle I \rangle < 18.0$ only if they are older and more luminous on the upper MS. Alternatively, in order to see a system with $\tau < 0.2\tau_{\rm MS}$ and $\langle I \rangle < 18.0$, the primary must be rather massive with $M_1 \gtrsim 6\,\rm M_\odot$. Note that all of our observed eclipsing binaries with reflection effects have early B-type MS primaries with $M_1 \gtrsim 6\,\rm M_\odot$. Because the IMF is significantly weighted toward lower-mass primaries, our magnitude-limited sample is dominated by late-B primaries that are systematically older on the upper MS. This is the reason why the probability of observing a young system with $\tau < 0.2\,\tau_{\rm MS}$ in our magnitude-limited sample is only $\mathcal{P}_\tau \approx 0.08$.

Putting these three factors together, then the probability of observing reflection effects is $\mathcal{P}_{\rm refl} = \mathcal{P}_i\,\mathcal{P}_\tau\,\mathcal{P}_P \approx 0.8\%$. In our actual sample, we selected $\mathcal{N}_{\rm B}$ = 174,000 B-type MS stars from the OGLE-III LMC survey. From this population, we observed $\mathcal{N}_{\rm obs} = 19$ eclipsing binaries that exhibit reflection effects with q = 0.06 - 0.25 companions and P = 3.0 - 8.5 days. After accounting for the correction factor $\mathcal{F}_{\rm Opik} = 1.23$ due to the Öpik effect, then the intrinsic fraction of B-type MS stars with low-mass q = 0.06 - 0.25 companions and short orbital periods P = 3.0 - 8.5 days is $F = (\mathcal{N}_{\rm obs}\,\mathcal{F}_{\rm Opik})\,/\,(\mathcal{N}_{\rm B}\,\mathcal{P}_{\rm refl}) \approx (19 \times 1.23)\,/\,(174{,}000 \times 0.008) \approx 1.7\%$. This is only an approximation as we need to quantify $\mathcal{P}_{\rm refl}$ as a function of q in a more robust manner. Nonetheless, this simple analysis separates the individual selection effects and illustrates the difficulty in detecting young, low-mass pre-MS companions that eclipse B-type MS stars.

5.3. *Detailed Monte Carlo Simulation*

We now perform a more detailed Monte Carlo simulation by synthesizing NIGHTFALL light curves for a population of eclipsing binaries. Using our probability density functions, we select a binary with a primary mass M_1, mass ratio q, age τ, and dust extinction A_I. Based on our adopted evolutionary stellar tracks, we then determine the observed magnitude $\langle I \rangle$ and color $\langle V - I \rangle$ of the binary. If the magnitudes and colors do not satisfy our photometric selection criteria, we generate a new binary. Otherwise, we count its contribution toward our statistics of binaries with B-type MS primaries. For each of the four mass-ratio bins, we simulate $\mathcal{N}_{\rm sim} = 2{\times}10^4$ binaries that satisfy our magnitude and color criteria and therefore have B-type MS primaries.

For each of these binaries, we then select P, t_o, i, and A_2 according to their respective probability density functions. To be detectable as a detached, closely orbiting eclipsing binary, the system must be old enough so that the pre-MS companion neither fills its Roche lobe nor accretes from a thick circumstellar disk (see §2). Based on our observed systems (Table 2), we therefore require the companion Roche-lobe fill-factor to be $RLFF_2 < 80\%$ and the age $\tau > 0.5$ Myr. If these criteria are satisfied, we synthesize an eclipsing binary light curve with NIGHTFALL as in §3.2 according to our eight randomly generated physical model parameters. We note that we have implicitly assumed that the orbital periods of binaries do not significantly change between $\tau = 0.5$ Myr and the time $\tau \approx \tau_{\rm MS} \approx 25$ Myr until the primary fills its Roche lobe. It is possible, however, that subsequent dynamical interactions with a tertiary can harden the orbit of the inner binary (Kiseleva et al. 1998; Naoz & Fabrycky 2014). This may bring additional systems into our parameter space P = 3.0 - 8.5 days after the secondary has contracted into a MS star. Hence, we can only measure the fraction of B-type MS stars with close, low-mass companions at 0.5 Myr $\lesssim \tau \lesssim 0.4\ \tau_{\rm MS} \approx 10$ Myr. The binary fraction at earlier or later epochs may be different.

We now ensure our synthesized light curve matches the cadence and precision of the OGLE-III LMC observations. We therefore interpolate our theoretical NIGHTFALL eclipsing binary light curve at $\mathcal{N}_I = 470$ randomly selected orbital phases. Obviously, the total photometric errors increase toward fainter systems. We relate the I-band photometric error to the I-band magnitude according to the following:

$$\sigma_{\rm fit}(I) = \left[1 + 10^{(I-17.0)/2}\right] \times 0.0072\,{\rm mag}. \qquad (10)$$

This simple formula fits the observed rms scatter in the eclipsing binary light curves as discussed in §2.1 (see black curve in Fig. 2). For each I-band value in our

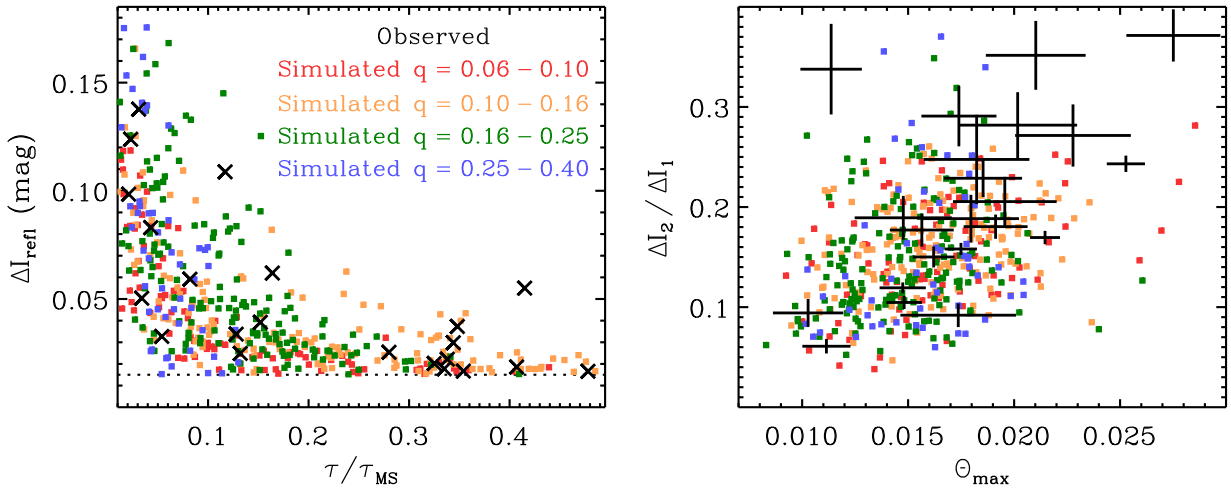

FIG. 11.— We compare the properties of the 22 observed eclipsing binaries (black) to the 468 simulated systems (color) with B-type MS primaries, low-mass $q = 0.06$ - 0.40 pre-MS companions, and pronounced reflection effects as listed in Table 5. Left panel: The anti-correlation between the reflection effect amplitude and the age relative to the MS lifetime of the primary is similar to the trend seen in the middle panel of Fig 9. Binaries with moderate mass ratios $q = 0.25$ - 0.40 (blue) can have pre-MS companions only at extremely young ages $\tau \lesssim 0.1\ \tau_{\rm MS}$, while lower-mass companions can have pre-MS evolutions that last up to ≈50% the MS lifetime of the primary. Right panel: Identical parameter space used in Fig. 3 to identify our systems and differentiate them from other classes of eclipsing binaries. Our simulated systems correspond well to the observed population. We can therefore easily identify eclipsing binaries with B-type MS primaries and low-mass pre-MS companions at $P = 3.0$ - 8.5 days by selecting systems with reflection effect amplitudes $\Delta I_{\rm refl} > 0.015$ mag, maximum eclipse widths $\Theta_{\rm max} < 0.03$, and ratios of eclipse depths $\Delta I_2/\Delta I_1 < 0.4$.

synthesized light curve, we add random Gaussian noise according to Eq. 10.

We then fit our analytic model of Gaussians and sinusoids (Eq. 3) to this simulated I-band light curve by implementing the same Levenberg-Marquardt technique in §2.1. To ensure automated and fast convergence toward the true solution, we choose initial model parameters motivated by the properties of the eclipsing binary. For example, because we only synthesize eclipsing binaries with circular orbits in our Monte Carlo simulations, we select $\Phi_2 = 0.5$ as the initial estimates in our analytic models. In this manner, for each synthetic eclipsing binary generated by NIGHTFALL, we measure the analytic model parameters, e.g. ΔI_1, Θ_1, $\Delta I_{\rm refl}$, etc., and their respective errors.

To be considered an eclipsing binary with observable reflection effects, we impose the same selection criteria as in §2. The reflection effect amplitude must be $\Delta I_{\rm refl} > 0.015$ mag with a 1σ error that is <20% the actual value. We require the uncertainties in the eclipse depths ΔI_1 and ΔI_2 and eclipse widths Θ_1 and Θ_2 to be <25% their respective values. The full light curve amplitude $\Delta I = \Delta I_1 + \Delta I_{\rm refl}$ must be deep enough to be detectable by the OGLE-III LMC survey according to Eq. 6. Finally, the maximum eclipse width $\Theta_{\rm max} < 0.03$ and ratio of eclipse depths $\Delta I_2/\Delta I_1 < 0.4$ need to satisfy our selected parameter space as shown in Fig. 3. If the synthetic light curve satisfies all these properties, then it contributes toward the number $\mathcal{N}_{\rm refl}$ of eclipsing binaries with reflection effects.

5.4. *Results*

We generated a total of $4 \times \mathcal{N}_{\rm sim} = 8{\times}10^4$ eclipsing binaries with B-type MS primaries, low-mass companions $q = 0.06$ - 0.40, and magnitudes and colors that satisfy our photometric selection criteria. Of these simulated systems, only $\mathcal{N}_{\rm refl} = 468$ eclipsing binaries have the necessary ages and orientations to produce detectable reflection effects and eclipses. We compare the properties of these $\mathcal{N}_{\rm refl} = 468$ eclipsing binaries from our Monte Carlo simulations to our 22 observed systems in Fig. 11. In the left panel, we can see that larger reflection effect amplitudes dictate younger relative ages $\tau/\tau_{\rm MS}$ for both the observed and simulated populations. The only system that noticeably deviates from this trend is ID-18330, which has a moderate reflection effect $\Delta I_{\rm refl} = 0.056$ and older relative age $\tau/\tau_{\rm MS} = 0.42$. We note that ID-18330 has a large intrinsic V-band scatter $f_{\sigma,V} = 3.0$ and a modest fit statistic $\chi^2/\nu = 1.16$, so that the systematic error in our measured age for this system is larger than usual. In any case, ID-18330 is relatively bright $\langle I \rangle = 16.1$, which requires a massive primary $M_1 \approx 15\,{\rm M}_\odot$. Hence, ID-18330 has a large relative age $\tau/\tau_{\rm MS} = 0.42$ mainly because the massive primary is short-lived with $\tau_{\rm MS} \approx 13\,{\rm Myr}$. We therefore expect the majority of eclipsing binaries with $\tau/\tau_{\rm MS} > 0.2$ to have $\Delta I_{\rm refl} < 0.04$ mag, while only the few systems with short-lived, massive primaries $M_1 \gtrsim 14\,{\rm M}_\odot$ can have $\Delta I_{\rm refl} \approx 0.04$ - 0.06 mag at these older relative ages.

In the right panel of Fig. 11, we compare the maximum eclipse depths $\Theta_{\rm max}$ versus the ratio of eclipse depths $\Delta I_2/\Delta I_1$ for our 468 simulated and 22 observed eclipsing binaries. Both the observed and simulated systems cluster near $\Theta_{\rm max} = 0.017$ and $\Delta I_2/\Delta I_1 = 0.2$. As discussed in §2, the pre-MS companions are detached from their Roche lobes and have low luminosities, which require $\Theta_{\rm max} < 0.3$ and $\Delta I_2/\Delta I_1 < 0.4$, respectively. Only the three systems at the top with $0.3 < \Delta I_2/\Delta I_1 < 0.4$ are marginally discrepant with the simulated population. Two of these, ID-1965 and ID-6630, have reflection effect amplitudes $\Delta I_{\rm refl} = 0.017$ - 0.019 mag just above our detection limit of $\Delta I_{\rm refl} = 0.015$ mag and companion properties that are consistent with the zero-age MS (see Fig. 6). If we had assumed a detection limit of $\Delta I_{\rm refl} = 0.012$ mag in our Monte Carlo simulations, we would have

Table 5. Results of Monte Carlo simulation.

$\log q$	q	$\mathcal{N}_{\rm obs}$	$\mathcal{N}_{\rm refl}$	$\mathcal{P}_{\rm refl}$ (%)	F (%)
−1.2 - −1.0	0.06 - 0.10	5	92	0.46	0.77 ± 0.34
−1.0 - −0.8	0.10 - 0.16	8	156	0.78	0.73 ± 0.26
−0.8 - −0.6	0.16 - 0.25	6	167	0.84	0.51 ± 0.21
−0.6 - −0.4	0.25 - 0.40	2	53	0.26	0.53 ± 0.37
−1.2 - −0.6	**0.06 - 0.25**	**19**	**415**	**0.69**	$\mathbf{2.0 \pm 0.6}$

synthesized an additional ≈15% of reflecting eclipsing binaries. The majority of these additional systems would have occupied the upper-right portion in the right panel of Fig. 11, consistent with ID-1965 and ID-6630. The other eclipsing binary, ID-17217, that is slightly discrepant with the simulated population has a slightly asymmetric light curve profile between eclipses (see Fig. 5). This asymmetry is most likely due to an eccentric orbit, as indicated by the phase of the secondary eclipse $\Phi_2 = 0.490$. However, the slight asymmetry could also be caused by a disk or hot spot, similar to other systems we observed with $\Delta I_2/\Delta I_1 > 0.4$ (see Fig. 3). Even if this one system is a contaminant in our sample, it has a negligible effect on our statistics. Most importantly, the 19 observed eclipsing binaries with $\Delta I_2/\Delta I_1 < 0.3$ match the simulated population and clearly have young, low-mass companions.

We present the statistics of our Monte Carlo simulations in Table 5. For each of our four mass-ratio intervals, we report the number $\mathcal{N}_{\rm obs}$ of observed systems in our sample, the number $\mathcal{N}_{\rm refl}$ of simulated systems that exhibit reflection effects, the probability of observing reflection effects $\mathcal{P}_{\rm refl} = \mathcal{N}_{\rm refl}/\mathcal{N}_{\rm sim}$ where $\mathcal{N}_{\rm sim} = 2{\times}10^4$, and the intrinsic binary fraction $F = (\mathcal{N}_{\rm obs}\,\mathcal{F}_{\rm Opik})\,/\,(\mathcal{N}_{\rm B}\,\mathcal{P}_{\rm refl})$ where $\mathcal{F}_{\rm Opik} = 1.23$ and $\mathcal{N}_{\rm B} = 174{,}000$. As expected, $\mathcal{P}_{\rm refl} \approx 0.8\%$ is largest for systems with $q = 0.10$ - 0.25. The probability $\mathcal{P}_{\rm refl} \approx 0.3\%$ quickly diminishes toward larger mass ratios because the pre-MS timescales of more massive companions are markedly shorter. Even though lower mass companions $q = 0.06$ - 0.10 have longer pre-MS evolutions, the probability $\mathcal{P}_{\rm refl} \approx 0.5\%$ of observing eclipses and reflection effects is low because the radii of the companions are systematically smaller (see Figs. 4 and 6).

In the bottom row of Table 5, we combine the statistics for our three smallest mass-ratio bins. For our observed sample of 19 eclipsing binaries in this interval, the relative error from Poisson statistics is 23%. We expect a systematic error of 15% due to uncertainties in our light curve modeling. For example, the few systems with $q = 0.20$ - 0.25 could easily shift toward solutions with $q > 0.25$ outside our defined interval of extreme mass ratios. We also estimate a 10% systematic error due to third light contamination and the possibility of mimics in our sample. For example, ID-5898 may have $q < 0.25$ and should therefore be added to our statistics (see §3), while ID-17217 may host a disk and/or hot spot and therefore should be removed from our statistics (see above). Finally, the correction factor $\mathcal{F}_{\rm Opik}$ due to the Öpik effect is uncertain by 10%. We add all these sources of error in quadrature, and find the total relative error in our binary statistics is ≈30%. Therefore, $F = (2.0 \pm 0.6)\%$ of young B-type MS stars have low-mass companions $q = 0.06$ - 0.25 with short orbital periods $P = 3.0$ - 8.5 days. This result from our detailed Monte Carlo simulation is consistent with our simple estimate of $F \approx 1.7\%$. The selection effects are therefore well understood and the probability of observing reflection effects is robust.

6. DISCUSSION

6.1. *Binary Statistics*

The close binary fraction of MS stars has long been understood to increase with primary mass (Abt 1983; Duquennoy & Mayor 1991; Raghavan et al. 2010; Sana et al. 2012; Duchêne & Kraus 2013). This correlation between the close binary fraction and spectral type has been primarily based on observations of moderate mass-ratio companions with $q \gtrsim 0.25$. In Fig. 12, we show the binary star fraction across orbital periods $P = 3.0$ - 8.5 days as a function of mass ratio q for solar-type primaries (Grether & Lineweaver 2006), B-type primaries (Wolff 1978; Levato et al. 1987; Abt et al. 1990), and O-type primaries (Sana et al. 2012). About 1.0% of solar-type stars have companions with moderate mass ratios $q > 0.25$ and short orbital periods $P = 3.0$ - 8.5 days. This increases to $\approx 3.8\%$ for B-type MS stars, and up to $\approx 14\%$ for O-type stars. Hence, the close binary fraction at moderate mass ratios $q > 0.25$ increases by a factor of ≈ 4 between $M_1 \approx 1\,{\rm M}_\odot$ solar-type primaries and $M_1 \approx 10\,{\rm M}_\odot$ B-type MS primaries.

As discussed in §1, SB1s with early-type MS primaries may have companions that are evolved stellar remnants (Wolff 1978; Garmany et al. 1980). We can therefore not reliably infer the frequency of extreme mass-ratio stellar companions from early-type spectroscopic binaries. The companions in our reflecting eclipsing binaries are unambiguously low-mass, unevolved, pre-MS stars. After correcting for geometrical and evolutionary selection effects (§5), we found that $(2.0 \pm 0.6)\%$ of young B-type MS stars have companions with $q = 0.06$ - 0.25 and $P = 3.0$ - 8.5 days. Considering 3.8% of B-type MS stars have companions with $q > 0.25$ across the same period range, then extreme mass-ratio companions $q = 0.06$ - 0.25 constitute one-third of close stellar companions to B-type MS stars. This result indicates the majority of SB1s with B-type MS primaries contain low-mass stellar companions. This is in disagreement with Wolff (1978), who suggested SB1s with late-B MS primaries most likely contain white dwarf companions.

For solar-type MS primaries $M_1 \approx 1\,{\rm M}_\odot$, low-mass companions $M_2 \approx 0.1$ - $0.2\,{\rm M}_\odot$ are almost certainly low-mass M-dwarfs (Duquennoy & Mayor 1991; Halbwachs et al. 2000). In a sample of 2,001 spectroscopic binaries with solar-type MS primaries (Grether & Lineweaver 2006), only 4 (0.2%) had companions with $P = 3.0$ - 8.5 days and $q \approx 0.08$ - 0.25. We found that $(2.0 \pm 0.6)\%$ of B-type MS stars have stellar companions across the same mass-ratio and period interval, which is a factor of ≈10 times larger (Fig. 12). The frequency of close, extreme-mass ratio companions increases with primary mass even more dramatically than the overall close binary fraction.

We can also interpret this trend according to differences in the intrinsic mass-ratio probability distribution p_q. The mass-ratio distribution is typically described by a power-law $p_q \propto q^\gamma\,dq$. For close

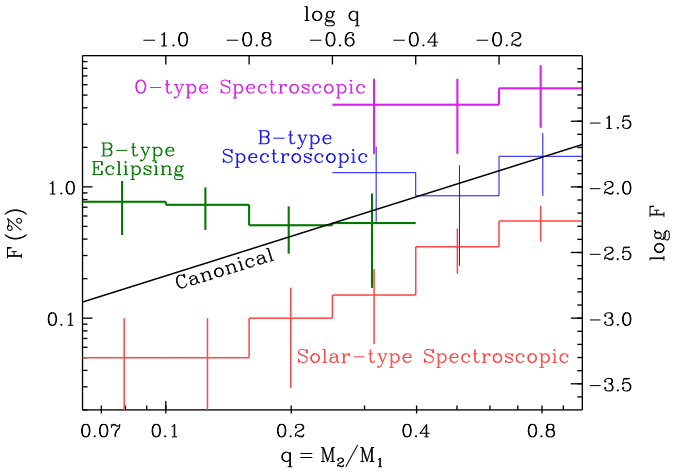

FIG. 12.— The fraction F of MS primaries that have stellar companions with orbital periods P = 3.0 - 8.5 days divided into $d\log q = 0.2$ intervals. In a spectroscopic survey of 71 O-type stars (magenta; Sana et al. 2012) and combined sample of 234 B-type stars (blue; Wolff 1978; Levato et al. 1987; Abt et al. 1990), 10 (14%) and 9 (3.8%), respectively, were identified as double-lined spectroscopic binaries in our period range with dynamically measured mass ratios $q > 0.25$. Utilizing eclipsing binaries is the only way of accurately measuring the intrinsic frequency of low-mass unevolved stellar companions to B-type MS stars (green). In a survey of 2,001 solar-type primaries (Grether & Lineweaver 2006), only 25 (1.2%) were found to be spectroscopic binaries in our period range with mass functions that indicate a stellar secondary companion with $q > 0.08$ (red). Population synthesis studies of close binaries canonically assume a uniform mass-ratio distribution (Kiel & Hurley 2006; Ruiter et al. 2011; Claeys et al. 2014), i.e. flat in *linear* q, according to $dF = 0.1\,dq\,d\log P$ (black).

companions to solar-type MS stars, the mass-ratio distribution across $0.08 < q < 1.0$ is close to uniform, i.e. $\gamma = 0.1 \pm 0.2$ (Grether & Lineweaver 2006; Raghavan et al. 2010). By combining the statistics of eclipsing binaries and SB2s with B-type MS primaries, we measure $\gamma = -0.7 \pm 0.3$ across the broad interval $0.07 < q < 1.0$ (Fig. 12). This is consistent with our previous measurement of $\gamma = -0.8 \pm 0.3$ in Moe & Di Stefano (2013) for close companions (P = 2 - 20 days) to B-type MS stars. In Moe & Di Stefano (2013), however, we used only the primary eclipse depth distribution of eclipsing binaries to recover the intrinsic mass-ratio distribution. In the present study, we have directly measured the physical properties of companions with extreme mass ratios q = 0.07 - 0.25. Not only does the close binary fraction increase with primary mass, but the mass-ratio distribution also becomes weighted toward smaller values (see also Duchêne & Kraus 2013, and references therein).

6.2. *Binary Formation*

The dearth of short-period, low-mass companions to solar-type MS stars has been investigated in previous spectroscopic binary surveys (Duquennoy & Mayor 1991; Halbwachs et al. 2003; Raghavan et al. 2010). In fact, there appears to be a complete absence of close $q \approx 0.02$ - 0.08 companions to solar-type MS stars, commonly known as the brown dwarf desert (Halbwachs et al. 2000; Grether & Lineweaver 2006). This is most likely because such low-mass companions would have migrated inward during their formation in the circumstellar disk and subsequently merged with the primary (Armitage & Bonnell 2002). For luminous and massive B-type MS primaries, however, the circumstellar disk quickly photoevaporates within $\tau \lesssim 0.3$ Myr (Alonso-Albi et al. 2009). Moreover, B-type MS stars with $q \approx 0.1$ companions have ≈10 times more mass and orbital angular momenta than their solar-type counterparts. Our nascent eclipsing binaries demonstrate that the rapid disk photoevaporation timescales and larger orbital angular momenta of more massive binaries can allow an extreme mass-ratio system to stabilize into a short orbit without necessarily merging.

As discussed in §1, there is a body of work indicating that components in close binaries coevolved via fragmentation and competitive accretion in the circumbinary disk (Bate & Bonnell 1997; Bate et al. 2002; Bonnell & Bate 2005; Kratter & Matzner 2006). Coevolution preferentially leads to binary component masses that are correlated. The rapid disk photoevaporation timescales around more massive stars suggest competitive accretion may be less significant. It is therefore plausible that less efficient competitive accretion in early-type systems can naturally produce close binaries with extreme mass ratios. This would be consistent with the measured mass-ratio distribution of close early-type binaries, which favors extreme mass ratios more readily than that observed for solar-type binaries.

It is also possible that extreme mass-ratio binaries require a different formation mechanism. The low-mass pre-MS companions in our eclipsing binaries are quite large with moderate Roche-lobe fill-factors $30\% < RLFF_2 < 80\%$. Tidal dissipation of orbital energy and angular momentum in a pre-MS star with a large convective envelope is orders of magnitude more efficient than in a MS star (Zahn & Bouchet 1989). Binary formation via tidal capture of low-mass companions may be substantially more efficient than previously realized (Press & Teukolsky 1977; Moeckel & Bally 2007) if one accounts for the long pre-MS timescales of the low-mass secondaries. Additionally, the pre-MS companions may have been captured with the assistance of dynamical perturbations from an outer tertiary via Kozai cycles and tidal friction (Kiseleva et al. 1998; Naoz & Fabrycky 2014). In any case, future formation models of massive stars and close binaries must readily produce these kinds of systems on rapid timescales.

6.3. *Binary Evolution*

Given the short orbital periods $P < 10$ days of our 22 systems, we expect these binaries will eventually coalesce as the primary evolves off the MS. Low-mass X-ray binaries and millisecond pulsars that form in the galactic field (Kalogera & Webbink 1998; Kiel & Hurley 2006) as well as Type Ia supernovae that explode in elliptical galaxies (Whelan & Iben 1973; Ruiter et al. 2011) can derive from B-type MS primaries with low-mass companions $q \approx 0.1$ - 0.3 at slightly longer orbital periods $P \approx 10^2$ - 10^3 days. These binary population synthesis studies canonically assume a uniform mass-ratio distribution, i.e. $\gamma = 0$, normalized to 0.1 companions per primary per decade of orbital period (Fig. 12). We have shown that low-mass companions

$q < 0.25$ to B-type MS stars at short orbital periods $P < 10$ days not only survive, but are found in abundance and constitute one-third of such close companions (i.e., $\gamma \approx -0.7$).

Photometrically resolved companions to early-type MS stars with $P \gtrsim 10^5$ days are generally weighted toward even smaller mass ratios (Preibisch et al. 1999; Shatsky & Tokovinin 2002; Peter et al. 2012). These wide companions to early-type stars may have formed relatively independently from the primaries, and may therefore have a mass-ratio distribution exponent $\gamma = -2.35$ that is consistent with random pairings from a Salpeter IMF (Abt et al. 1990; Duchêne et al. 2001).

If we interpolate between these two regimes, then we may expect low-mass companions to early-type stars to be plentiful at moderate orbital periods. Hence, there may be more progenitors of low-mass X-ray binaries, millisecond pulsars, and Type Ia supernovae than originally assumed. We intend to confirm this conjecture by investigating the properties of massive binaries at intermediate orbital separations. Specifically, we are in the process of characterizing OGLE-III LMC eclipsing binaries with B-type MS primaries and $P > 20$ days (Moe et al., in prep.).

7. SUMMARY

1. *New Class of Eclipsing Binaries.* We analyzed the light curves of 2,206 systems in the OGLE-III LMC eclipsing binary catalog (Graczyk et al. 2011) with B-type MS primaries and orbital periods $P = 3\text{-}15$ days (§2.1). We discovered a subset of 22 detached eclipsing binaries with short orbital periods ($P = 3.0\text{-}8.5$ days) that exhibit substantial reflection effects ($\Delta I_{\rm refl} = 0.017\text{-}0.138$ mag) and moderate to deep primary eclipses ($\Delta I_1 = 0.09\text{-}2.8$ mag). Because such deep eclipses and prominent reflection effects require the secondaries to be comparable in size to the primaries ($R_2/R_1 > 0.3$) but markedly cooler ($T_2/T_1 < 0.4$), we concluded the companions in these 22 eclipsing binaries are large, cool, low-mass pre-MS stars (§2.2).

   Similar irradiation effects have been observed in evolved binaries that contain a hot, low-luminosity, compact remnant in an extremely short orbit ($P \lesssim 1$ day) with a late-type MS companion (§2.3.1). Previous observations of young MS + pre-MS eclipsing binaries have been limited to large mass ratios $q \gtrsim 0.5$, low-mass primaries $M_1 \lesssim 3\,{\rm M}_\odot$, and/or systems that are still accreting from a circumbinary disk (§2.3.2). Hence, our 22 eclipsing binaries constitute a new class of nascent eclipsing binaries in which a detached, non-accreting, low-mass pre-MS companion discernibly reflects much of the light it intercepts from the B-type MS primary. We have not yet observed the precise counterparts to these systems in our own Milky Way galaxy, primarily because our sample of continuously monitored $\mathcal{N}_{\rm B} = 174{,}000$ B-type MS stars in the OGLE-III LMC dataset (Udalski et al. 2008) is two orders of magnitude larger than previous surveys.

2. *Physical Model Fits.* For detached eclipsing binaries with MS primaries and known distances, we can utilize stellar evolutionary tracks to estimate the ages τ and component masses M_1 and M_2 based solely on the observed photometric light curves (§3.1 - 3.2). For the 18 definitive MS + pre-MS eclipsing binaries, we measured primary masses $M_1 = 6\text{-}16\,{\rm M}_\odot$, secondary masses $M_2 = 0.8\text{-}2.4\,{\rm M}_\odot$ ($q = 0.07\text{-}0.36$), and ages $\tau = 0.6\text{-}8$ Myr (§3.3). We investigated multiple sources of systemic uncertainties and performed various consistency checks (§3.4). Our conclusions that the majority of our reflecting eclipsing binaries have pre-MS companions with extreme mass ratios $q < 0.25$ and young ages $\tau < 8$ Myr are robust.

3. *Association with H II Regions.* Relative to our total sample of 2,206 B-type MS eclipsing binaries, the coordinates of our 22 reflecting eclipsing binaries are correlated with the positions of star-forming H II regions at the 4.1σ significance level (§4). In addition, our youngest eclipsing binaries with deeper eclipses and larger reflection effect amplitudes are more likely to be associated with bright and/or compact H II regions. These statistics and correlations: (1) reinforce our conclusions that our reflecting eclipsing binaries contain young, low-mass, pre-MS companions, (2) demonstrate the reliability of our eclipsing binary models, and (3) provide powerful diagnostics for the expansion velocities $\langle v \rangle_{\rm H\,II} \approx 10\text{-}30$ km s^{-1} and long-term dynamical evolution of H II regions.

4. *Intrinsic Close Binary Statistics.* We performed detailed Monte Carlo simulations to generate synthetic light curves for a large population of eclipsing binaries (§5.1 - 5.3). Only $\mathcal{P}_{\rm refl} \approx 0.7\%$ of B-type MS stars with low-mass companions have the necessary ages and orientations to produce detectable eclipses and reflection effects (§5.4). Hence, $F = (2.0 \pm 0.6)\%$ of B-type MS stars have companions with extreme mass ratios $q = 0.06\text{-}0.25$ and short orbital periods $P = 3.0\text{-}8.5$ days. This is $\approx$10 times larger than that observed around solar-type MS stars in the same period and mass-ratio interval (§6.1). Our analysis represents the first direct measurement for the fraction of B-type MS stars with close, low-mass, non-degenerate stellar companions.

5. *Implications for Binary Formation.* The lack of close extreme mass-ratio companions to solar-type MS stars, commonly known as the brown dwarf desert, is probably because such companions migrated inward at the time of formation in the circumbinary disk and merged with the primary (Armitage & Bonnell 2002). Because massive binaries have rapid disk photoevaporation timescales and larger orbital angular momenta, our extreme mass-ratio eclipsing binaries could therefore stabilize into short orbits without merging (§6.2). Close binaries with extreme mass ratios may have formed either through: (1) less efficient competitive accretion in the circumbinary disk (Bate & Bonnell 1997), (2) tidal capture while the secondary is still a large, convective pre-MS star (Press & Teukolsky 1977; Moeckel & Bally 2007), and/or (3) Kozai cycles with a tertiary component and subsequent tidal friction between the inner B-type MS + low-mass pre-MS inner binary (Kiseleva et al. 1998).

6. *Implications for Binary Evolution.* B-type MS stars with closely orbiting low-mass companions $q = 0.1$ - 0.3 can evolve to produce Type Ia supernovae, low-mass X-ray binaries, and millisecond pulsars (Kiel & Hurley 2006; Ruiter et al. 2011). We find more close, low-mass companions to B-type MS stars than is typically assumed in binary population synthesis (§6.3). If this result holds at slightly longer orbital periods, we anticipate more progenitors of Type Ia supernovae and low-mass X-ray binaries than originally predicted.

This research was funded by the National Science Foundation under grant AST-1211843. We acknowledge use of publicly available data from the Optical Gravitational Lensing Experiment (Udalski et al. 2008; Graczyk et al. 2011) and the Magellanic Cloud Emission Line Survey (Smith et al. 2005). We thank the referee, A. Prša, for helpful comments and suggestions that improved the quality of the manuscript. We alo thank N. Evans, J. Najita, S. Naoz, C. Badenes, I. Czekala, C. Faesi, and D. Nelson for useful discussions.

REFERENCES

Abt, H. A. 1983, ARA&A, 21, 343
Abt, H. A., Gomez, A. E., & Levy, S. G. 1990, ApJS, 74, 551
Abt, H. A., Levato, H., & Grosso, M. 2002, ApJ, 573, 359
Alecian, E., Goupil, M.-J., Lebreton, Y., Dupret, M.-A., & Catala, C. 2007, A&A, 465, 241
Alonso-Albi, T., Fuente, A., Bachiller, R., Neri, R., Planesas, P., Testi, L., Berné, O., & Joblin, C. 2009, A&A, 497, 117
Armitage, P. J. & Bonnell, I. A. 2002, MNRAS, 330, L11
Bally, J. & Zinnecker, H. 2005, AJ, 129, 2281
Barlow, B. N., Kilkenny, D., Drechsel, H., Dunlap, B. H., O'Donoghue, D., Geier, S., O'Steen, R. G., Clemens, J. C., LaCluyze, A. P., Reichart, D. E., Haislip, J. B., Nysewander, M. C., & Ivarsen, K. M. 2013, MNRAS, 430, 22
Bate, M. R. & Bonnell, I. A. 1997, MNRAS, 285, 33
Bate, M. R., Bonnell, I. A., & Bromm, V. 2002, MNRAS, 336, 705
Belczynski, K., Kalogera, V., Rasio, F. A., Taam, R. E., Zezas, A., Bulik, T., Maccarone, T. J., & Ivanova, N. 2008, ApJS, 174, 223
Bertelli, G., Nasi, E., Girardi, L., & Marigo, P. 2009, A&A, 508, 355
Bica, E. L. D., Schmitt, H. R., Dutra, C. M., & Oliveira, H. L. 1999, AJ, 117, 238
Bond, H. E. 2000, in Astronomical Society of the Pacific Conference Series, Vol. 199, Asymmetrical Planetary Nebulae II: From Origins to Microstructures, ed. J. H. Kastner, N. Soker, & S. Rappaport, 115
Bonnell, I. A. & Bate, M. R. 2005, MNRAS, 362, 915
Cardelli, J. A., Clayton, G. C., & Mathis, J. S. 1989, ApJ, 345, 245
Casey, B. W., Mathieu, R. D., Vaz, L. P. R., Andersen, J., & Suntzeff, N. B. 1998, AJ, 115, 1617
Chu, Y.-H. & Kennicutt, Jr., R. C. 1994, Ap&SS, 216, 253
Cichowolski, S., Romero, G. A., Ortega, M. E., Cappa, C. E., & Vasquez, J. 2009, MNRAS, 394, 900
Claeys, J. S. W., Pols, O. R., Izzard, R. G., Vink, J., & Verbunt, F. W. M. 2014, A&A, 563, A83
Claret, A. 2001, MNRAS, 327, 989
Crowther, P. A. 2013, MNRAS, 428, 1927
de Marchi, F., Poretti, E., Montalto, M., Piotto, G., Desidera, S., Bedin, L. R., Claudi, R., Arellano Ferro, A., Bruntt, H., & Stetson, P. B. 2007, A&A, 471, 515
de Wit, W. J., Testi, L., Palla, F., Vanzi, L., & Zinnecker, H. 2004, A&A, 425, 937
Devor, J. & Charbonneau, D. 2006, ApJ, 653, 647
Devor, J., Charbonneau, D., O'Donovan, F. T., Mandushev, G., & Torres, G. 2008, AJ, 135, 850
di Criscienzo, M., Ventura, P., & D'Antona, F. 2009, A&A, 496, 223
Dotter, A., Chaboyer, B., Jevremović, D., Kostov, V., Baron, E., & Ferguson, J. W. 2008, ApJS, 178, 89
Duchêne, G. & Kraus, A. 2013, ARA&A, 51, 269
Duchêne, G., Simon, T., Eislöffel, J., & Bouvier, J. 2001, A&A, 379, 147
Duquennoy, A. & Mayor, M. 1991, A&A, 248, 485
Ekström, S., Meynet, G., Chiappini, C., Hirschi, R., & Maeder, A. 2008a, A&A, 489, 685
Ekström, S., Meynet, G., Maeder, A., & Barblan, F. 2008b, A&A, 478, 467
Evans, N. R., DeGioia-Eastwood, K., Gagné, M., Townsley, L., Broos, P., Wolk, S., Nazé, Y., Corcoran, M., Oskinova, L., Moffat, A. F. J., Wang, J., & Walborn, N. R. 2011, ApJS, 194, 13
Fitzpatrick, E. L. 1999, PASP, 111, 63
Garmany, C. D., Conti, P. S., & Massey, P. 1980, ApJ, 242, 1063
Graczyk, D., Soszyński, I., Poleski, R., Pietrzyński, G., Udalski, A., Szymański, M. K., Kubiak, M., Wyrzykowski, Ł., & Ulaczyk, K. 2011, Acta Astron., 61, 103
Grebel, E. K. & Chu, Y.-H. 2000, AJ, 119, 787
Grether, D. & Lineweaver, C. H. 2006, ApJ, 640, 1051
Gullikson, K. & Dodson-Robinson, S. 2013, AJ, 145, 3
Halbwachs, J. L., Arenou, F., Mayor, M., Udry, S., & Queloz, D. 2000, A&A, 355, 581
Halbwachs, J. L., Mayor, M., Udry, S., & Arenou, F. 2003, A&A, 397, 159
Hall, D. S. & Garrison, Jr., L. M. 1969, PASP, 81, 771
Harris, J. & Zaritsky, D. 2009, AJ, 138, 1243
Hartmann, L. 2009, Accretion Processes in Star Formation: Second Edition (Cambridge University Press)
Hillenbrand, L. A. & White, R. J. 2004, ApJ, 604, 741
Howarth, I. D. 2013, A&A, 555, A141
Hubrig, S., Le Mignant, D., North, P., & Krautter, J. 2001, A&A, 372, 152
Hut, P. 1981, A&A, 99, 126
Iben, Jr., I. & Tutukov, A. V. 1987, ApJ, 313, 727
Indu, G. & Subramaniam, A. 2011, A&A, 535, A115
Kallrath, J. & Milone, E. F. 2009, Eclipsing Binary Stars: Modeling and Analysis
Kalogera, V. & Webbink, R. F. 1998, ApJ, 493, 351
Kiel, P. D. & Hurley, J. R. 2006, MNRAS, 369, 1152
Kiseleva, L. G., Eggleton, P. P., & Mikkola, S. 1998, MNRAS, 300, 292
Klagyivik, P., Csizmadia, S., Pasternacki, T., Fruth, T., Erikson, A., Cabrera, J., Chini, R., Eigmüller, P., Kabath, P., Kirste, S., Lemke, R., Murphy, M., Rauer, H., & Titz-Weider, R. 2013, ApJ, 773, 54
Kobulnicky, H. A. & Fryer, C. L. 2007, ApJ, 670, 747
Korn, A. J., Becker, S. R., Gummersbach, C. A., & Wolf, B. 2000, A&A, 353, 655
Kouwenhoven, M. B. N., Brown, A. G. A., Portegies Zwart, S. F., & Kaper, L. 2007, A&A, 474, 77
Kratter, K. M. & Matzner, C. D. 2006, MNRAS, 373, 1563
Lee, J. W., Kim, S.-L., Kim, C.-H., Koch, R. H., Lee, C.-U., Kim, H.-I., & Park, J.-H. 2009, AJ, 137, 3181
Levato, H. & Grosso, M. 2013, PASP, 125, 1191
Levato, H., Malaroda, S., Morrell, N., & Solivella, G. 1987, ApJS, 64, 487
Massey, P. & Hunter, D. A. 1998, ApJ, 493, 180
Mathieu, R. D. 1994, ARA&A, 32, 465
Mazeh, T. & Goldberg, D. 1992, ApJ, 394, 592
Mazeh, T., Goldberg, D., Duquennoy, A., & Mayor, M. 1992, ApJ, 401, 265
Mazeh, T., Tamuz, O., & North, P. 2006, MNRAS, 367, 1531
Miszalski, B., Acker, A., Moffat, A. F. J., Parker, Q. A., & Udalski, A. 2009, A&A, 496, 813
Moe, M. & Di Stefano, R. 2013, ApJ, 778, 95
Moeckel, N. & Bally, J. 2007, ApJ, 656, 275

Morales-Calderón, M., Stauffer, J. R., Stassun, K. G., Vrba, F. J., Prato, L., Hillenbrand, L. A., Terebey, S., Covey, K. R., Rebull, L. M., Terndrup, D. M., Gutermuth, R., Song, I., Plavchan, P., Carpenter, J. M., Marchis, F., García, E. V., Margheim, S., Luhman, K. L., Angione, J., & Irwin, J. M. 2012, ApJ, 753, 149
Naoz, S. & Fabrycky, D. C. 2014, ArXiv e-prints
Ngeow, C.-C. & Kanbur, S. M. 2005, MNRAS, 360, 1033
Nordstrom, B. & Johansen, K. T. 1994, A&A, 282, 787
O'Dell, C. R., Henney, W. J., Abel, N. P., Ferland, G. J., & Arthur, S. J. 2009, AJ, 137, 367
Öpik, E. 1923, Publications of the Tartu Astrofizica Observatory, 35, 6
Paczyński, B. 1971, ARA&A, 9, 183
Palla, F. & Stahler, S. W. 1990, ApJ, 360, L47
—. 2001, ApJ, 553, 299
Parker, R. J. & Goodwin, S. P. 2007, MNRAS, 380, 1271
Pecaut, M. J. & Mamajek, E. E. 2013, ApJS, 208, 9
Perryman, M. A. C., Lindegren, L., Kovalevsky, J., Hoeg, E., Bastian, U., Bernacca, P. L., Crézé, M., Donati, F., Grenon, M., Grewing, M., van Leeuwen, F., van der Marel, H., Mignard, F., Murray, C. A., Le Poole, R. S., Schrijver, H., Turon, C., Arenou, F., Froeschlé, M., & Petersen, C. S. 1997, A&A, 323, L49
Peter, D., Feldt, M., Henning, T., & Hormuth, F. 2012, A&A, 538, A74
Phinney, E. S. & Kulkarni, S. R. 1994, ARA&A, 32, 591
Pietrukowicz, P., Mróz, P., Soszyński, I., Udalski, A., Poleski, R., Szymański, M. K., Kubiak, M., Pietrzyński, G., Wyrzykowski, A., Ulaczyk, K., Kozłowski, S., & Skowron, J. 2013, Acta Astron., 63, 115
Pietrzyński, G., Graczyk, D., Gieren, W., Thompson, I. B., Pilecki, B., Udalski, A., Soszyński, I., Kozłowski, S., Konorski, P., Suchomska, K., Bono, G., Moroni, P. G. P., Villanova, S., Nardetto, N., Bresolin, F., Kudritzki, R. P., Storm, J., Gallenne, A., Smolec, R., Minniti, D., Kubiak, M., Szymański, M. K., Poleski, R., Wyrzykowski, Ł., Ulaczyk, K., Pietrukowicz, P., Górski, M., & Karczmarek, P. 2013, Nature, 495, 76
Podsiadlowski, P. 1991, Nature, 350, 136
Popper, D. M. 1987, ApJ, 313, L81
Preibisch, T., Balega, Y., Hofmann, K.-H., Weigelt, G., & Zinnecker, H. 1999, New Astronomy, 4, 531
Press, W. H. & Teukolsky, S. A. 1977, ApJ, 213, 183
Prša, A., Guinan, E. F., Devinney, E. J., DeGeorge, M., Bradstreet, D. H., Giammarco, J. M., Alcock, C. R., & Engle, S. G. 2008, ApJ, 687, 542
Prša, A. & Zwitter, T. 2005, ApJ, 628, 426
Raghavan, D., McAlister, H. A., Henry, T. J., Latham, D. W., Marcy, G. W., Mason, B. D., Gies, D. R., White, R. J., & ten Brummelaar, T. A. 2010, ApJS, 190, 1
Reid, W. A. & Parker, Q. A. 2010, MNRAS, 405, 1349
Ritter, H., Zhang, Z.-Y., & Kolb, U. 2000, A&A, 360, 969
Rizzuto, A. C., Ireland, M. J., Robertson, J. G., Kok, Y., Tuthill, P. G., Warrington, B. A., Haubois, X., Tango, W. J., Norris, B., ten Brummelaar, T., Kraus, A. L., Jacob, A., & Laliberte-Houdeville, C. 2013, MNRAS, 436, 1694
Ruiter, A. J., Belczynski, K., Sim, S. A., Hillebrandt, W., Fryer, C. L., Fink, M., & Kromer, M. 2011, MNRAS, 417, 408
Sana, H., de Mink, S. E., de Koter, A., Langer, N., Evans, C. J., Gieles, M., Gosset, E., Izzard, R. G., Le Bouquin, J.-B., & Schneider, F. R. N. 2012, Science, 337, 444
Shatsky, N. & Tokovinin, A. 2002, A&A, 382, 92
Siess, L., Dufour, E., & Forestini, M. 2000, A&A, 358, 593
Smith, R. C., Points, S. D., Chu, Y.-H., Winkler, P. F., Aguilera, C., Leiton, R., & MCELS Team. 2005, in Bulletin of the American Astronomical Society, Vol. 37, American Astronomical Society Meeting Abstracts, 1200
Stassun, K. G., Mathieu, R. D., Cargile, P. A., Aarnio, A. N., Stempels, E., & Geller, A. 2008, Nature, 453, 1079
Stelzer, B., Huélamo, N., Hubrig, S., Zinnecker, H., & Micela, G. 2003, A&A, 407, 1067
Taam, R. E. & Sandquist, E. L. 2000, ARA&A, 38, 113
Tognelli, E., Prada Moroni, P. G., & Degl'Innocenti, S. 2011, A&A, 533, A109
Tohline, J. E. 2002, ARA&A, 40, 349
Tokovinin, A., Thomas, S., Sterzik, M., & Udry, S. 2006, A&A, 450, 681
Tomita, A., Ohta, K., Nakanishi, K., Takeuchi, T. T., & Saito, M. 1998, AJ, 116, 131
Udalski, A., Soszynski, I., Szymanski, M. K., Kubiak, M., Pietrzynski, G., Wyrzykowski, L., Szewczyk, O., Ulaczyk, K., & Poleski, R. 2008, Acta Astron., 58, 89
Verbunt, F. 1993, ARA&A, 31, 93
Whelan, J. & Iben, Jr., I. 1973, ApJ, 186, 1007
Wilson, R. E. 1972, Ap&SS, 19, 165
Windemuth, D., Herbst, W., Tingle, E., Fuechsl, R., Kilgard, R., Pinette, M., Templeton, M., & Henden, A. 2013, ApJ, 768, 67
Wolff, S. C. 1978, ApJ, 222, 556
Yorke, H. W. 1986, ARA&A, 24, 49
Zahn, J.-P. & Bouchet, L. 1989, A&A, 223, 112
Zaritsky, D. 1999, AJ, 118, 2824
Zaritsky, D., Harris, J., Thompson, I. B., & Grebel, E. K. 2004, AJ, 128, 1606